UNIVERSITE DE LIMOGES

ECOLE DOCTORALE Science et Ingénierie en Matériaux Mécanique Energétique et Aéronautique (SI-MMEA)

Groupe d'Etude des Matériaux Hétérogènes (GEMH)

N°

Thèse

Présentée pour obtenir le grade de

DOCTEUR DE L'UNIVERSITE DE LIMOGES

Discipline / Spécialité : Matériaux Céramiques et Traitements de surface

par

Emilie DAHLEM

Présentée et soutenue le 20 Décembre 2011 à Leoben (Autriche)

CHARACTERISATION OF REFRACTORY FAILURE UNDER COMBINED HYDROSTATIC AND SHEAR LOADING AT ELEVATED TEMPERATURES

Thèse dirigée par : Marc HUGER et Thierry CHOTARD

JURY:

Rapporteurs

M. T.CUTARD	Maître-Assistant HDR	ICA-Albi, Mines d'Albi
M. H. HARMUTH	Professeur des universités	Chair of Ceramics, Montanuniversität (Autriche)

Examinateurs

M. T. CHOTARD	Professeur des universités	GEMH, Université de Limoges
M. M. HUGER	Professeur des universités	GEMH, ENSCI
M. P. O'LEARY	Professeur des universités	Chair of Automation, Montanuniversität (Autriche)

Affidavit

I declare in lieu of oath, that I wrote this thesis and performed the associated research myself, using only literature cited in this volume.

Acknowledgements

The financial support by the Austrian Federal Government (in particular from the Bundesministerium für Verkehr, Innovation und Technologie and the Bundesministerium für Wirtschaft und Arbeit) and the Styrian Provincial Government, represented by Österreichische Forschungsförderungsgesellschaft mbH and by Steirische Wirtschaftsförderungsgesellschaft mbH, within the research activities of the K2 Competence Centre on “Integrated Research in Materials, Processing and Product Engineering”, operated by the Materials Center Leoben Forschung GmbH in the framework of the Austrian COMET Competence Centre Programme, is gratefully acknowledged. Furthermore I received personal promotion by FIRE (The Federation for International Refractory Research and Education). Special thanks to Michel RIGAUD, Professor Emeritus École Polytechnique, University of Montréal, Canada, FIRE Executive Secretary.

I want to express my sincere gratitude to my thesis supervisors, o.Univ. Prof. Dipl.-Ing. Dr. mont. Harald Harmuth, Dipl.-Ing. Dr. mont. Dietmar Gruber and Dipl.-Ing. Dr. mont. Thomas Auer from the University of Leoben and Prof. Dr. Ing. Thierry Chotard and Prof. Dr. Ing. Marc Huger from the University of Limoges and ENSCI (Ecole Nationale Supérieure de Céramique Industrielle) respectively, for their friendship and guidance throughout the duration of this work.

I thank Univ.-Prof.Dipl.-Ing.Dr.mont. Thomas Antretter for his help and tips for using the software ABAQUS.

Furthermore, I would like to thank the GEMH (Groupe d’étude des Matériaux Hétérogènes) team of Egletons, Mr. Christophe Petit, Ms Anne Millien and Mr. Ion-Octavian Pop which allowed me to use their “Double shear test” device for my work.

I would like to thank all laboratory technicians of University of Leoben.

Lastly and most importantly, I would like to thank my family. My father Alain, my mother Bernadette, my sister Céline and her fiancé Julien for their role in encouraging me to attain this goal.

A mon père Alain, ma mère Bernadette,

ma sœur Céline et son fiancé Julien,

ma marraine Martine et mon oncle Eugène

mes grands-parents

Table of content

PROBLEM DEFINITION

For finite element simulation application, material behavior needs to be taken into account at room temperature and at elevated temperatures. Material laws and testing methods already exist for Mode I failure.

If the material has a fracture in Mode II or III or a mixed mode including additional compressive forces, suitable material laws exist. One solution is to use the Drucker-Prager criterion. This is a classical approach describing the dependence of shear stress in dependence of the hydrostatic pressure. It necessitates the determination of material parameters like friction angle and cohesion. Testing methods to determine these parameters are available for room temperature only, testing methods are missed for elevated temperatures.

Presently applied testing methods for application of material laws like Drucker-Prager or Mohr-Coulomb use a triaxial test cell which applies a hydraulic pressure on a polymer sleeve. This equipment suitable for room temperature cannot be applied for elevated temperatures, as it would be necessary for refractories. Therefore the main goal of the present thesis is to develop suitable testing methods. These should be applied to refractory materials with rather different mechanical behavior. Moreover attempts should be made to verify these newly develop testing procedures. The investigations performed should include necessary Finite Element Analysis.

CHAPTER 1: STATE OF THE ART – LITERATURE

I INTRODUCTION

Refractory materials in use are subjected to stress which is necessary to consider in order to choose the adequate materials. The knowledge of the behavior under load is important for a comprehension of the mechanisms likely to cause failure and to determine the mechanical properties for numerical modeling.

This section firstly reports a small and concise synthesis according to the standard and physical techniques currently applied to characterize the mechanical properties of refractories.

Secondly, a presentation of the different material failure criteria will be given. Attention will be paid on criteria which are more dedicated to heterogeneous materials (industrial refractory materials are heterogeneous) specifically submitted to combined state of stress (for example shear and compression in combination). Finally, a listing of existing shear tests will be presented. The need for a new design of shear tests according to specific requests (characterization under combined stress state at elevated temperatures) coming from either the experimental or the simulation side of the design process will be emphasized.

II THERMO-MECHANICAL PROPERTIES

For more than a century, standard tests have been used to provide information concerning the behavior of refractory materials **[SCHA-04, PRIE-05]**. Engineers have started using tests originally developed for civil engineering like the modulus of rupture (MOR). As refractories are exposed to high temperatures during production process, this test method was adapted for elevated temperatures (HMOR). A new testing procedure which requires only one sample to sweep a whole temperature range was invented afterwards. The test is called refractoriness under load (RUL) and indicates the temperature at which the material softens. The RUL equipment may also be used for the creep in compression test (CIC). This test delivers the shrinkage of a refractory under constant load and exposed to a constant temperature over several hours.

Recently, the use of finite element simulation has become common in many fields of engineering sciences. Numerical simulation has been established in many areas such as the steel industry, a huge consumer of refractories. The numerical simulation helps to develop a new material or enhance its performance. Its advantage is to support understanding of mechanical and thermal behavior of refractory parts under service conditions. But the use of numerical simulation requires more than standard tests for definition of material parameters in order to use appropriate constitutive laws. The wedge splitting test and the tensile test have been introduced. The first one gives information on the work of fracture and the second one provides valuable information about the stress/stain behavior of the tested material.

II.1 Standard tests

II.1.1 Modulus of rupture (MOR)

The modulus of rupture (MOR) is the mechanical property most used for refractories. This test already existed in the 1800s to study the strength of wood. A parallelepipedic sample is bent until fracture using a three point flexural testing technique (Figure I-1). It represents the highest stress experienced within the material. This test can be adapted for the characterization at high temperatures, which defines the maximum stress in bending of hot material (hot modulus of rupture, HMOR, according to ASTM C-357, DIN 51048).

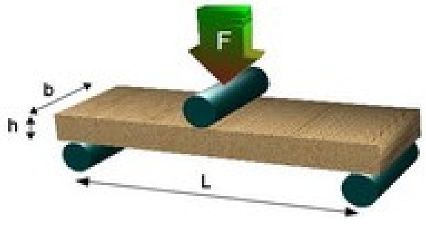

Figure I-1: Sketch of the three point bending test.

II.1.2 Refractoriness under load (RUL)

Refractoriness under load (RUL) is the refractory material property which measures resistance to a combined effect of heat and load **[SCHA-04, NETZ]**. This test was invented by K. Konopicky together with Toni Technik Company from Germany. For experiments, a cylindrical test sample (50 mm in diameter and height and with a co-axial bore of 12,5 mm) is subjected to a constant compressive load (0,2 MPa) and heated at a rate of 5°C/min until the maximum test temperature or until a particular percentage of deformation is reached (Figure I-2). Methods of measurement are detailed in DIN 51053/1 standard.

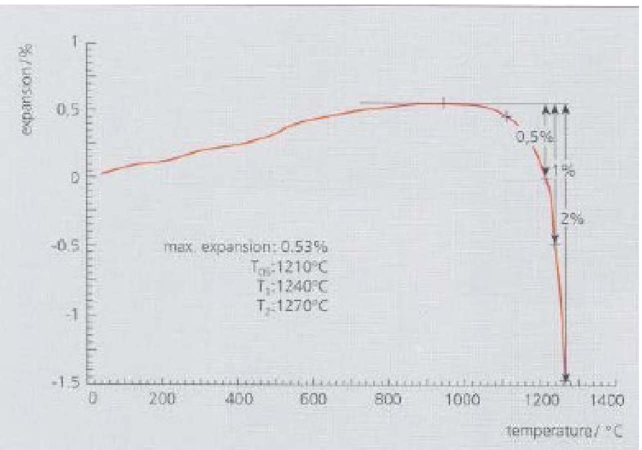

*Figure I-2: RUL test on a test piece taken from a fireclay brick **[NETZ]**.*

II.1.3 Creep in compression (CIC)

Creep in compression (CIC) **[SCHA-04, NETZ]** is described as the evolution of a deformation dependent on during which a refractory is under a specific compressive stress (DIN 51053/2) (Figure I-3).

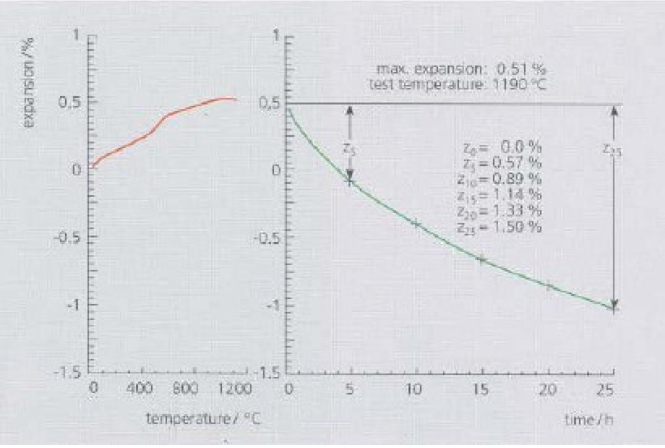

*Figure I-3: CIC test on a test piece taken from a fireclay brick **[NETZ]**.*

II.2 Non standard tests

II.2.1 Wedge splitting test (WST)

The material fracture energy is calculated from the load-displacement curve of this test. The WST was setup for concrete by Hillemeier and Hilsdorf **[HILL-77]**. A patent was appllied by Tschegg in 1986 **[TSCH-86]**. A WST is available at the Chair of Ceramics **[HARM-94, HARM-95, HARM-96, ANDR-03, NILI-05, TSCH-09]**. This device enables stable crack propagation and to study the non-linear fracture behavior of ordinary ceramic refractory materials and determine fracture energy. The WST (Figure I-4) is performed on notched shaped specimens which enable the determination of fracture energies of large fractured surfaces and even for materials exhibiting a rather brittle behavior.

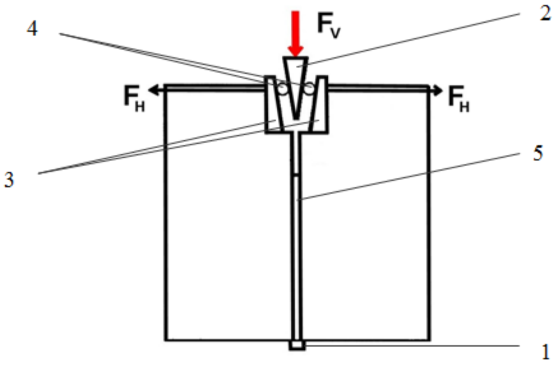

Figure I-4: Schematic sketch of the tested specimen: support (1), wedge (2), load transmission parts (3), rolls (4) starter notch (5).

F_V and F_H represent the vertical load of the testing machine and the horizontal component of the splitting force respectively. The crack starts from the starter notch and shows a stable propagation along the ligament.

II.3 Tensile test

Tensile test provides valuable information about the stress/strain behavior of the material. In addition, it allows the determination of the value of the Young's modulus. The testing device is available at the GEMH laboratory **[KAKR-07, BAHL-09]** (Figure I-6). Strain is measured by two extensometers equipped with silicon carbide rods placed on two opposite sides of the specimen. Refractory samples are constituted by a cylindrical rod (20 mm in diameter) with two metallic parts glued at each ends. The final geometry is manufactured by a lathe.

Tensile tests can be carried out, up to rupture, with either a constant stress velocity or a constant displacement velocity, with alternated load discharges. To determine the Young's modulus from tensile test results, the slope of the first loading step of the stress/strain curve is calculated.

Figure I-7 illustrates an example of determination of Young's modulus from the stress-strain curve (E_0). The specimen was tested by a tensile test at room temperature **[KAKR-07]**.

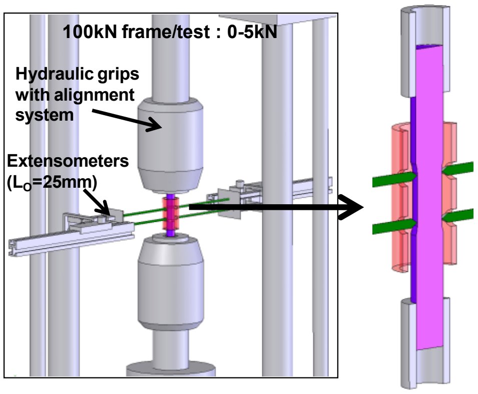

Figure I-5: Scheme of tensile test device.

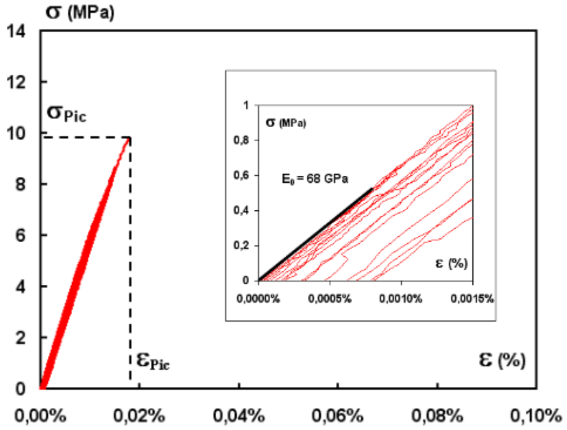

Figure I-6: Example of determination of Young's modulus from the stress-strain curve (E_0). Tensile test at room temperature in the case of castable specimen ***[KAKR-07]***.

III MATERIAL FAILURE CRITERIA

III.1 Principal stresses and stress invariants

The material failure criteria are especially applied to define failure under multiaxial compressive and shear loading. In order to avoid dependencies on the coordinate system loading is defined using stress invariants. The following quantities are used for this purpose:

σ_1, σ_2 and σ_3 are the principal stresses, where $\sigma_1 \geq \sigma_2 \geq \sigma_3$.

Mainly three invariants to define failure surfaces are used: I_1, J_2 and J_3. I_1 is the first invariant of the stress tensor; J_2 and J_3 are the second and the third invariant of the stress deviator tensor, respectively (Equations I-1 to I-3).

$$I_1 = \sigma_1 + \sigma_2 + \sigma_3 \tag{I-1}$$

$$J_2 = \frac{1}{6}\left[(\sigma_1 - \sigma_2)^2 + (\sigma_2 - \sigma_3)^2 + (\sigma_3 - \sigma_1)^2\right] \tag{I-2}$$

$$J_3 = (\sigma_1 - \sigma_m) \cdot (\sigma_2 - \sigma_m) \cdot (\sigma_3 - \sigma_m) \tag{I-3}$$

Where σ_m is the mean hydrostatic pressure:

$$\sigma_m = \frac{1}{3} \cdot I_1 \tag{I-4}$$

III.2 Multiaxial criteria

III.2.1 Development of existing criteria

III.2.1.a *Tresca criterion*

A simple yield criterion was proposed by Tresca **[OTTO-05, HOSF-05, COQU-05]**. The failure surface f is mathematically given by the equation:

$$f(\sigma_{ij}) = (\sigma_1 - \sigma_3) - 2 \cdot k = 0 \tag{I-5}$$

Where σ_1 and σ_3 represent the extreme principal stresses ($\sigma_1 \geq \sigma_2 \geq \sigma_3$) and k is a constant corresponding to the maximum shear strength (for cohesive soils, this parameter corresponds to the undrained shear strength c_u). Figure I-7 shows representations of the Tresca criterion in the deviatoric plane and in the principal stress space.

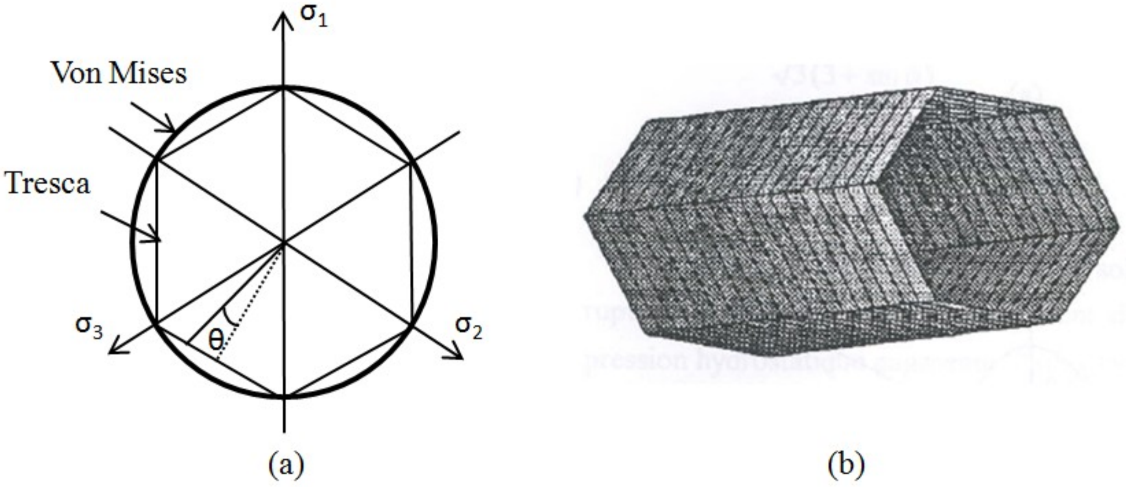

Figure I-7: Illustration of the Tresca criterion: (a) – in the deviatoric plane, (b) – in the principal stress space ***[LEE-94]****.*

III.2.1.b *Von Mises yield criterion*

To take into account the influence of the intermediate stress, Von Mises proposed that the failure surface depends on the second invariant of the deviatoric stress tensor, J_2 **[HOSF-05, LECK-09, COQU-05]**:

$$f(\sigma_{ij}) = \sqrt{J_2} - k = 0 \qquad \text{(I-6)}$$

Where k is a parameter of the constitutive law. It represents the strength of the material in pure shear. This criterion was developed to study metal behavior and it is not well adapted to the representation of soil behavior.

Figure I-8 shows representations of the Von Mises criterion in the deviatoric plane and in the principal stress space.

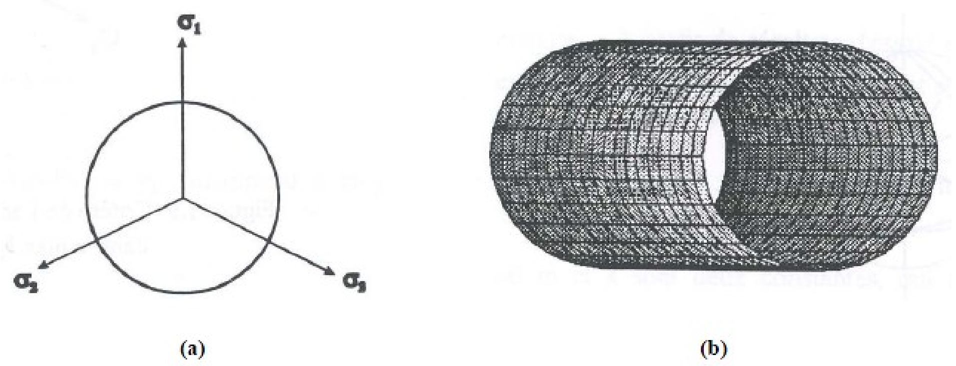

Figure I-8: Illustration of the Von Mises criterion: (a) – in the deviatoric plane, (b) – in the principal stress space ***[LEE-94]****.*

III.2.1.c *Mohr-Coulomb criterion*

The Coulomb criterion has served as a starting point for the majority of criteria used for geomaterials (soil, rock, concrete, backfill, etc). In its basic version, the Mohr-Coulomb criterion only uses two principal stresses, σ_1 and σ_3, with two basic material parameters, c (cohesion) and φ (internal friction angle). The theory of Mohr-Coulomb is used for granular soils (sands) and for long-term cohesive soils (clays and silts). **[AUBE-03, COQU-05]**. The failure surface $f(\sigma_{ij})$ is expressed as follows:

$$f(\sigma_{ij}) = (\sigma_1 - \sigma_3) - (\sigma_1 + \sigma_3) \cdot \sin\varphi - 2c \cdot \cos\varphi = 0 \tag{I-7}$$

When φ=0, we find the Tresca criterion.

Figure I-9 shows representations of the Mohr-Coulomb criterion in the deviatoric plane and in the principal stress space. The Coulomb criterion is linear in the I_1-$\sqrt{J_2}$ plane and it takes the form of an irregular hexagon in the plane of the octahedral stresses, with the axes of symmetry corresponding to the six summits of the Tresca criterion to which it is closely related in the π plane.

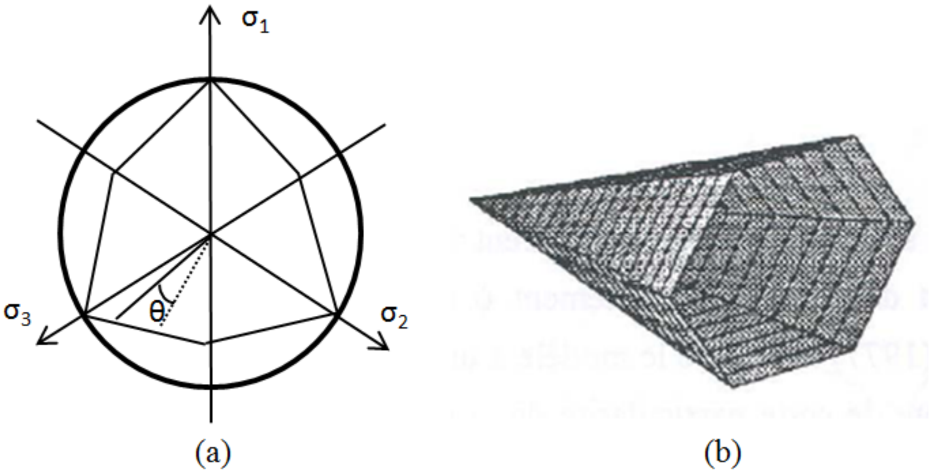

(a) (b)

Figure I-9: Illustration of the Mohr-Coulomb criterion:
(a) – in the deviatoric plane, (b) – in the principal stress space ***[LEE-94]***.

III.2.1.d ***Drucker-Prager criterion***

Drucker and Prager proposed a circular version of the Coulomb criterion in the octahedral plane (similar to von Mises criterion), while maintaining the linear relationship between I_1 and $\sqrt{J_2}$ (without a contribution from J_3).

The Drucker-Prager yield criterion is a pressure-dependent model for determining whether a material has undergone or failed plastic yielding **[NGUY-06, YU-10, COQU-05]**. The criterion was introduced to deal with the plastic deformation of soils. It and its many variants have been applied to rock, concrete, polymers, foams, and other pressure-dependent materials. The yield criterion for this class of materials is based on the shape of the yield surface in the meridional plane (Figure I-10).

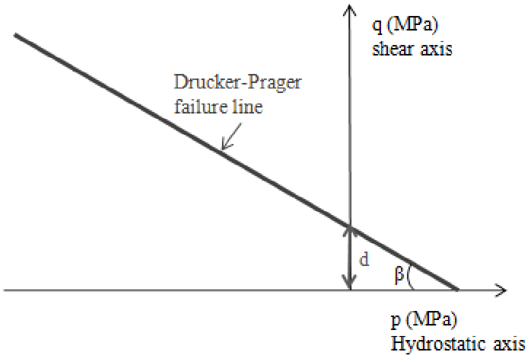

Figure I-10: Schematic representation of linear Drucker-Prager criterion.

The Drucker-Prager yield criterion is expressed as

$$q = -p \cdot \tan\beta + d$$
$$\sqrt{3 \cdot J_2} = -\frac{I_1}{3} \cdot \tan\beta + d \qquad \text{(I-8)}$$

The yield stress surface makes use of two invariants, defined as the equivalent pressure stress, $p = -\frac{1}{3} \cdot \mathrm{trace}(\sigma)$ and the Mises equivalent stress, $q = \sqrt{\frac{3}{2} \cdot (S:S)}$, where S is the stress deviator, defined as $S = \sigma + p \cdot I$.

Since the Drucker-Prager yield surface is a smooth version of the Mohr-Coulomb yield surface, it is often expressed in terms of the cohesion (c) and the angle of the internal friction (φ) that are used to describe the Mohr-Coulomb yield surface. If the Drucker-Prager yield surface circumscribes the Mohr-Coulomb yield surface then the relations become (Figure I-11, Equation I-9):

$$\tan\beta = \frac{\sqrt{3} \cdot \sin\varphi}{\sqrt{1 + \frac{1}{3} \cdot \sin^2\varphi}}$$
$$\frac{d}{c} = \frac{\sqrt{3} \cdot \cos\varphi}{\sqrt{1 + \frac{1}{3} \cdot \sin^2\varphi}} \qquad \text{(I-9)}$$

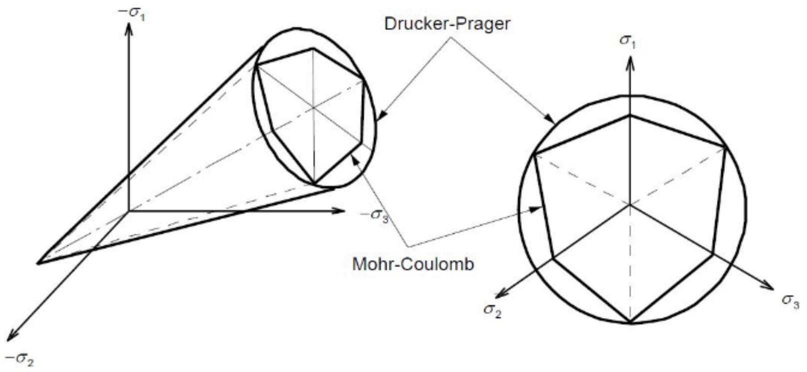

Figure I-11: The Mohr-Coulomb and the Drucker-Prager yield surfaces in principal stress coordinates.

III.2.1.e ***Hoek-Brown criterion***

The original Hoek-Brown failure criterion was developed during the preparation of the book “Underground Excavations in Rock” by E. Hoek and E.T. Brown, published in 1980 **[HOEK-80, BENZ-08, CLAU-08]**. It is probably the most widely used approach to represent the response of fractured rock to stress. This empirical relationship incorporates the degree of fracturing and rock alteration, among other factors, into a criterion.

$$\sigma'_1 = \sigma'_3 + \sigma_c \cdot \left(m \cdot \frac{\sigma'_3}{\sigma_c} + s\right)^a \tag{I-10}$$

$$\sigma'_1 = \sigma_1 + u \tag{I-11}$$

Where σ’$_1$ and σ’$_3$ are the maximum and minimum effective stresses at failure. Effective stress (σ’) acting on a soil is calculated from two parameters, total stress (σ) and pore water pressure (u) (Equation I-11). σ_c is the laboratory uniaxial compressive strength, and the empirical constants m and s are based on the rock mass quality. It is a classification of rock for engineering purposes, based on the number of major joints or other discontinuities (planes of weakness) in it, their orientation, and their spacing. The empirical constants are related in a general sense to the angle of internal friction of the rock mass (m) and the rock mass cohesive strength (s). For most hard-rock masses the constant a is equal to 0,5 and the equation is usually expressed in the following form:

$$\sigma'_1 = \sigma'_3 + \sqrt{m \cdot \sigma_c \cdot \sigma'_3 + s \cdot \sigma_c^2} \tag{I-12}$$

The parameters defining the Hoek-Brown criterion can be estimated from a combination of laboratory tests on intact rock cores and empirical adjustment to account for the reduced strength of the rock mass due to presence of discontinuities. The Figure I-12 illustrates the Hoek and Brown failure criterion in principal stress space and in the deviatoric plane.

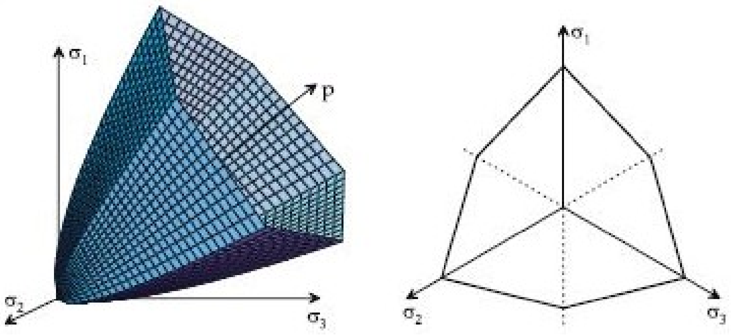

Figure I-12: Hoek and Brown failure criterion in principal stress space and in deviatoric plane.

IV EXISTING SHEAR TESTS

IV.1 Iosipescu shear test

The Iosipescu shear test was proposed by Iosipescu for determining shear properties of isotropic materials such as metals **[IOSI-67]** and has been studied extensively within the last 30 years **[BOTE-07, HAWO-04, KRIS-10, XAVI-04]**.

The Iosipescu specimen has the shape of a rectangular beam of small dimensions, with symmetric V-notches at its center (Figure I-13). The shear stress has a maximum value at the plane between the notch tips. A suitable fixture is used in order to transform the applied load into a shear loading, acting at the specimen minimum cross-section area, between the V-notches. The geometry of the V-notches is such that a quasi-uniform shear stress distribution is produced at the center of the specimen. The shear strains are usually measured with two-element rosette strain gauges, which average the stains over the area of the gauge grid. The rosettes are fixed at the center of the specimens at +/- 45° to their longitudinal axis. Linear and non-linear numerical analyses (both material and geometry) have been performed to improve the original V-notch shear test for application to composite systems.

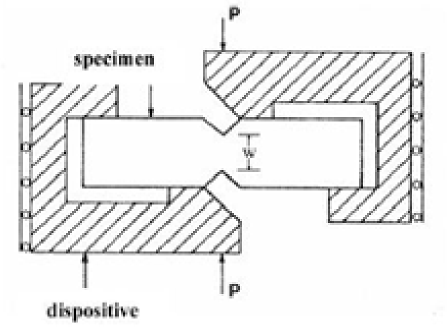

Figure I-13: Iosipescu test scheme.

The test device is able implementing quasi homogeneous stress on the shear surface. It is also possible by numerical modeling to calculate the angle of the stress path. But it is not easily possible to perform the test at elevated temperature. This test is principally used to analyze composite materials or woods.

IV.2 Inclined double notch shear test (IDNS)

The IDNS-concept uses the ASTM D 3864-specimen (test method for in-plane shear strength of reinforced plastic) and subjects it to a combination of loads. The specimen test region is confined by two notches cut perpendicular to the central interlaminar layer, one from each panel face. These notches serve as potential stress contractors. The IDNS-concept uses this intrinsic characteristic to create a state of nearly homogeneous interlaminar shear by minimization of the arising stress concentrations at the notch roots: this is accomplished by properly combining two load sets (normal loading N and bending M, see Figure I-14) with effects of opposing sign of notch near stress field **[MERL-00, PETT-06a, NEUM-, PETT-06b]**.

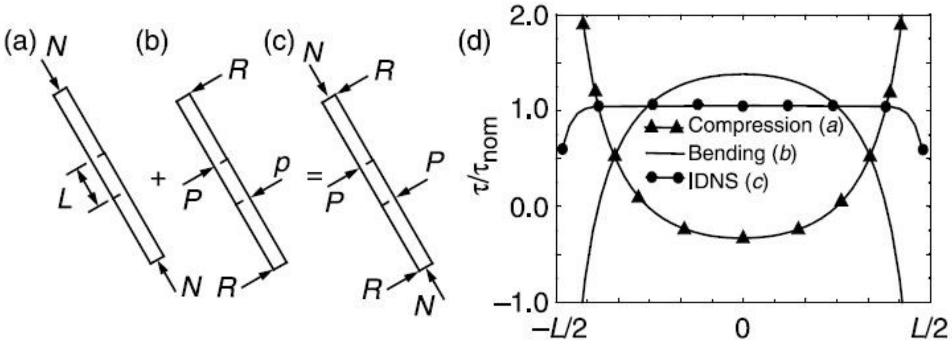

Figure I-14: Principal sketch of an IDNS loading concept: (a) normal compression, (b) bending and (c) properly superimposed combination. (d) Resulting FE-calculated shear stress profiles for the respective and properly combined load cases.

The testing device produces homogeneous stress on the shear surface of the sample. So it is possible by numerical modelisation of this method to calculate the angle of the stress path. But because of the complexity of the testing device, it is not possible to perform the test at elevated temperature. Furthermore this method uses a, by necessity, short specimen which is not suitable for refractory materials because of the grain size of up to 5 mm. This test is developed to determine shear properties of interlaminar samples in thin panels of layered composite materials.

IV.3 Multistage triaxial test

The multistage triaxial test (multiple failure states test) has been adopted as an alternative to a series of single-stage triaxial tests in order to establish material parameters like the cohesion and the friction angle. Whereas three single-stage triaxial tests are required to obtain a complete failure envelope, one multistage triaxial test may give the complete failure envelope **[YOUN-10].**

The multi-stage triaxial test concept was first introduced in the middle of the 1970s **[KOVA-75]** and was validated by comparing multi-stage triaxial test results with several single-stage triaxial test results **[KIM-79]**.

The used stress path involved applying an initial confining pressure followed by loading the sample until it shows beginning signs of failure. At that point the test is halted and the confining pressure is increased without removing the axial load. This procedure is repeated for as many confining pressures as required **[NORM-04]**.

This test is suitable for refractory materials giving a good approximation of the Drucker-Prager parameters but the use of hydraulic oil and rubber pressure sleeve during the test does not allow testing at elevated temperature.

V CONCLUSION

To predict the behavior of a refractory lining system, the knowledge of specific material properties characterizing combined shear/compressive failure is essential for finite elements simulations. The standard testing methods, developed for refractory materials (RUL, CIC, MOR, etc.) are insufficient for this purpose. The modeling step requires associated testing procedures.

Among several others such as Von Mises and Mohr- Coulomb, the Drucker-Prager material failure criterion has been found to be suitable to describe the complex state of loading in the most reliable way. Furthermore there is an unexhaustive listing of different available experimental devices. In order to be applied at elevated temperatures a testing procedure has to be developed.

CHAPTER 2:

DESIGN OF A NEW SHEAR TEST

I INTRODUCTION

The calculation of refractory lining failure requires for some cases the knowledge of multiaxial behavior under industrial conditions. The Drucker-Prager model has been chosen for this study and requires experimental determination of cohesion and friction angle parameters. This section of the work aims at proposing optimized specimen geometries through numerical simulation to determine the required parameters at elevated temperature.

Difficulties have been noticed in various studies on existing shear tests. The Iosipescu shear test is a testing device which is not able to be used at high temperature. Because of the complexity of the inclined double notch shear test, it is not possible to perform the test at elevated temperature.

II EXPERIMENTAL DETERMINATION OF THE DRUCKER-PRAGER CRITERION

The Drucker-Prager criterion can represent shear failure in refractory lining. It necessitates the definition of a straight line in the p-q space. To characterize this criterion it is necessary to determine two points. A first solution would be to have a first simple point for a zero hydrostatic pressure and a second point would be obtained by a combined loading compression-shear test (Figure II-1).

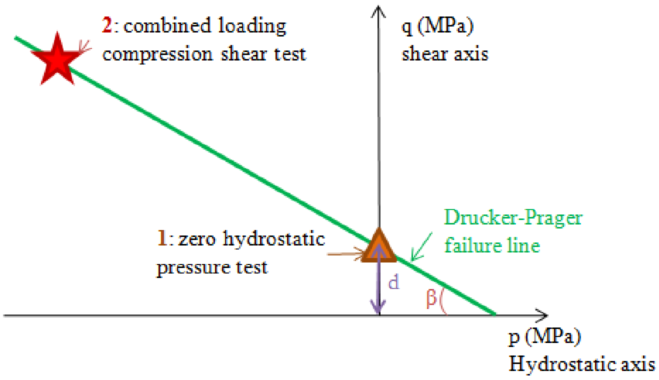

Figure II-1: Sketch of two points obtained by different tests allowing the characterization of the Drucker-Prager criterion.

At a point where the hydrostatic pressure is zero several solutions are possible. A first one is to use a double direct shear test with the geometry illustrated in Figure II-2 with uniaxial load. Some attempts were made, but unfortunately as bending tensile stress appears at the bottom of the two vertical notches, the results were not conclusive. As illustrated on Figure II-3, the fracture of such a geometry doesn't follow the vertical notches. Despite numerous efforts to improve the geometry by changing the size of the notches, no solution has been validated for a failure in pure shear mode.

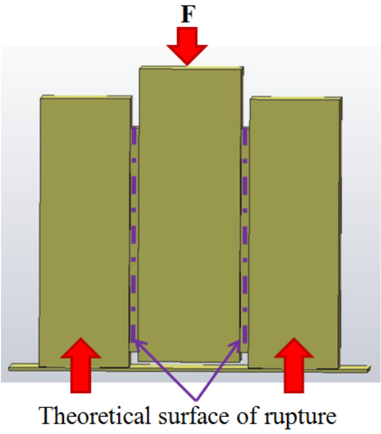

Figure II-2: Double direct shear test.

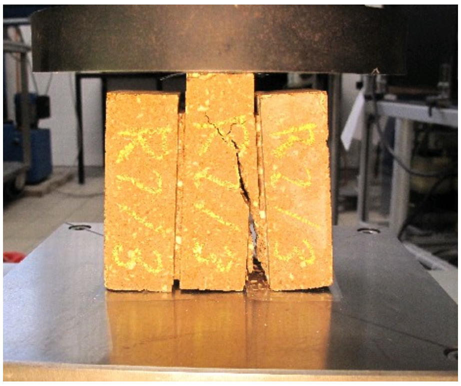

Figure II-3: Fracture of the double direct shear test.

A second approach is to use the same test principle as the previous double direct shear test with using an additional device to block the external sides of the geometry and allow the vertical displacement of the central part of the geometry as seen on Figure II-3. This kind of test limits the bending effect, which allows a rupture in shear mode. This test was initially developed for low temperatures, unfortunately it is not adaptable to test samples at elevated temperature.

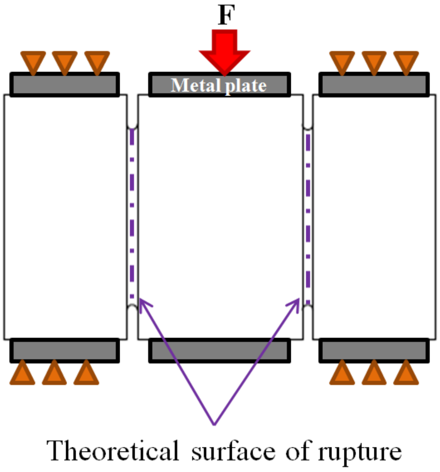

Figure II-4: Double direct shear test. *Figure II-5: Double direct shear test.*

Another possibility is the torsion test. This test presents some difficulties; the sample can slip in the two grips of the testing device which gives erroneous displacement data and the stress in the notch plane is not homogeneous thus causing problem to achieve the desired failure type. For the study a groove is machined in the middle of the specimen to guide the fracture (Figure II-6). The test is described in part IV.

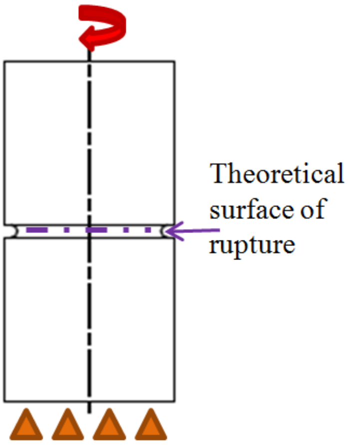

Figure II-6: Torsion test

The second point in the p-q space may be determined by a combined compression-shear test. A first solution would be to use a single stage triaxial test. The specimen enveloped carefully in the sleeve is kept in the triaxial cell and a desired lateral pressure is applied. Then the vertical load is increased until the specimen fails; that gives a point in the p-q diagram. Therefore, the tests should be carried out with at least two or three different lateral pressure values to find the values of the cohesion and the friction angle (Figure II-7 and Figure II-8). Unfortunately it is not possible to use this test at elevated temperature. More explanations of the testing procedure are given in part V.

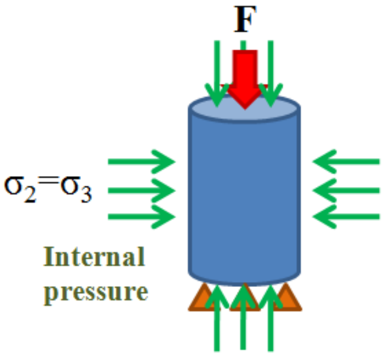

Figure II-7: Sketch of a triaxial test.

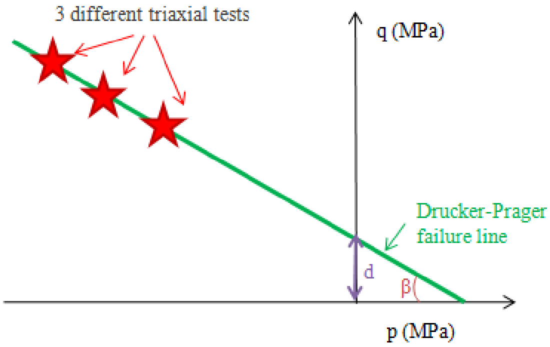

Figure II-8: p-q diagram obtained with 3 different triaxial tests.

A second possibility is to manufacture a notched bar specimen. It is uniaxially loaded and the fracture follows an inclined notch (Figure II-9 and Figure II-10). The specimen can be tested at elevated temperature. The angle of the stress path is determined by finite element simulation and with the combination of laboratory results, a point in the p-q diagram can be determined. This test is presented in the part III.

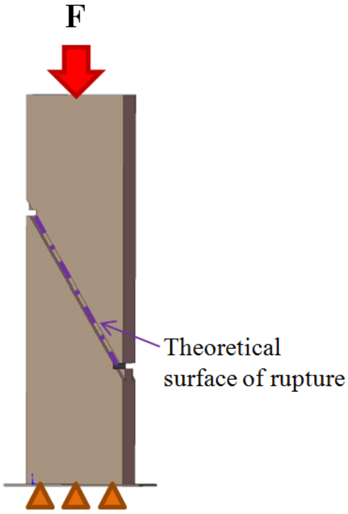

Figure II-9: Sketch of a uniaxial load of a notched bar specimen.

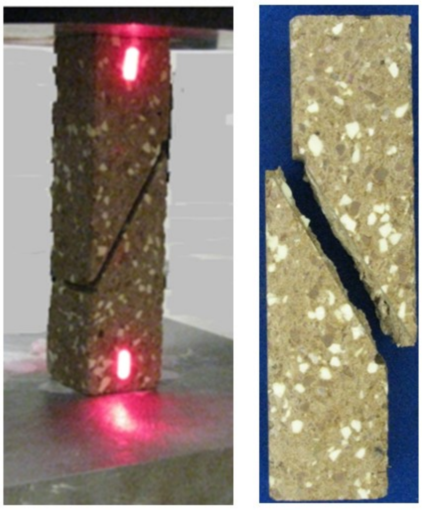

Figure II-10: Uniaxial load of a notched bar specimen and fractured sample.

A third solution is to use a torsion-compression test. Here the specimen is loaded uniaxially and subjected to torsion and can also be tested at elevated temperature. The determination of the angle of the stress path is achieved by finite element simulation and with the combination of laboratory results, a point in the p-q diagram can be drawn.

III MODIFIED SHEAR TEST

III.1 Un-notched bar specimen

To meet specifications quoted above, an un-notched bar specimen with the dimensions 150x37.5x37.5 mm^3 has been chosen.

At the beginning, specimen geometry was drawn with the software ABAQUS CAE (Figure II-11). One symmetrical quarter has been taken into account for numerical modeling to reduce the amount of calculation. The mesh type of the domain is performed using continuous elements of eight nodes with reduced integration (C3D8R). The model is deformable. The Young's modulus was fixed at 20 GPa and the Poisson's ratio to 0.3. The upper surface of the sample has an imposed vertical displacement of -1 mm along the y-axis to simulate a vertical load.

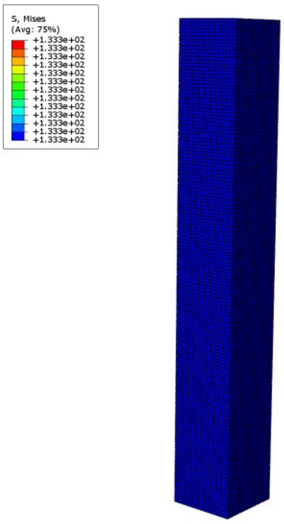

Figure II-11: FEM model of an un-notched shaped bar specimen.

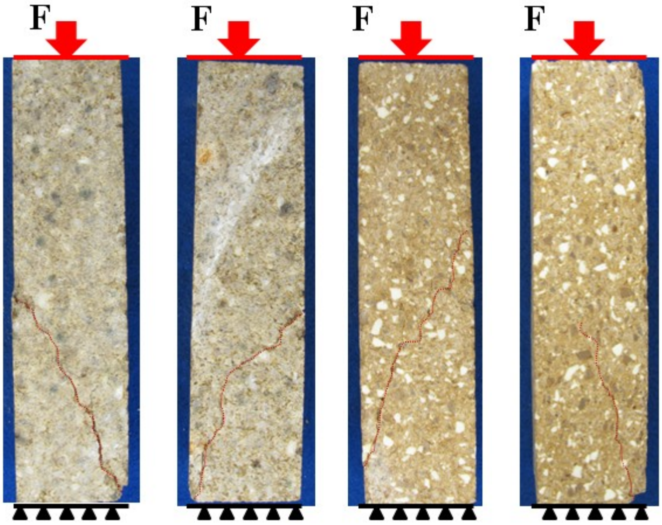

Figure II-12: Results of the uniaxial compression test of two un-notched bar specimen of each studied materials.

The simulation reveals that the Von Mises stress field is homogeneous through the entire specimen, so no stress concentration can be considered for crack onset. By the FEM simulation, the corresponding angle of the stress path in the p-q diagram is 71.56°.

Materials I and II (presented in part VII) were tested with a uniaxial compression testing device. The failure is not frank, not homogeneous and not repeatable Figure II-12. In order to achieved a reproducible shear failure it was decided to apply guided side notches. An angle of 60° was chosen for subsequent experiments at first.

III.2 60° single notch bar specimen

A specimen with the dimensions 150x37.5x37.5 mm^3 and a 60° inclined notch were depicted with ABAQUS CAE (Figure II-13). As the geometry is composed of two 60° inclined notches, only one symmetrical halve has been taken into account for numerical modeling. The major part of the meshing is performed using continuous elements with eight nodes with reduced integration (C3D8R). The mesh domain is uniformly distributed over the whole geometry and a finer mesh was used for the inclined notch. The Young's modulus was fixed at 20 GPa and the Poisson's ratio to 0.3. As in the previous case, the upper surface of the specimen has an imposed vertical displacement of -1 mm along the y-axis to simulate a vertical load.

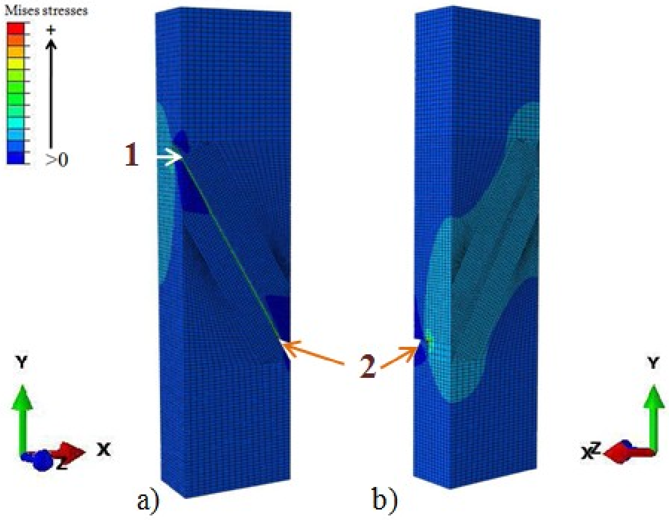

Figure II-13: Von Mises stresses of a bar specimen loaded vertically with a 60° inclined notch. a) front view, b) view at the plane of symmetry.

The simulation demonstrates that Von Mises stresses are not homogeneous through the entire specimen and are higher along the 60° inclined notch. However close to the center and at the end of the notches (points 1 and 2) a relatively large specimen volume shows increased Von Mises stresses. Therefore the side notches alone maybe not sufficient for crack guidance.

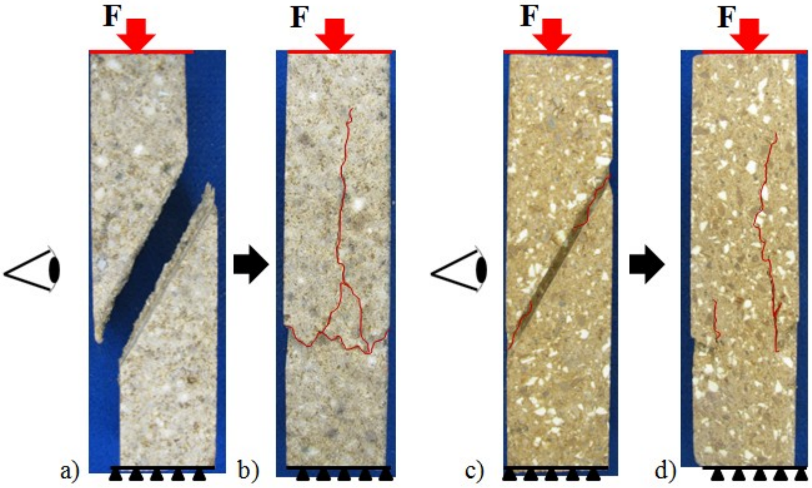

Figure II-14: Uniaxial compression test of a bar specimen with a 60° inclined notch. Front and side view (a and b) for material I; front and side view (c and d) for material II.

The samples of material I and II shown in Figure II-14 where tested with an uniaxial compression testing devise. For material I, the failure follows the inclined notch and the shear failure is smooth, but unpredictable vertical cracks appear on the opposite side of the specimen (Figure II-14b). At the unnotched faces for material II the failure follows the notch only close to its root. Inside the specimen it largely deviates from notch plain. Moreover similar to material I vertical cracks appear on the unnotched faces. To improve the fracture path additional notches have been machined as shown in the next section.

III.3 60° double notched bar specimens

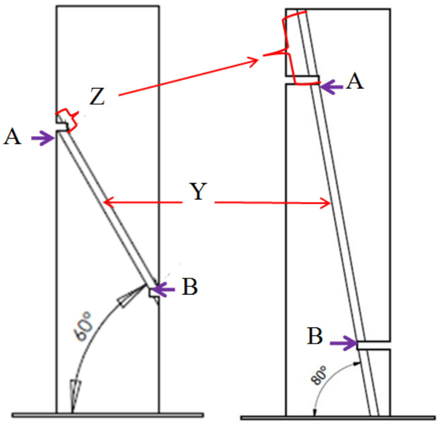

Figure II-15: Schema and denomination of the two different notches.

To guide the failure through the whole shear surface it is necessary to manufacture two different notches, i.e. one notch on each of the four lateral sides of the specimen.

Figure II-15 explains the different denominations that will be used for the modified shear test. Y represents the depth of the inclined notch. The horizontal notch is machined at a distance Z of the inclined notch. A-B is the length of the inclined notch.

III.3.1 Influence of different Y and Z dimensions

For optimization, finite element simulation is used. 9 combinations of the 60° inclined notched bar with the values of 5, 7.5, 10 mm for Y and 7, 7.5 and 10 mm for Z were studied (Table II-1).

For simulation, the aim is to obtain α (angle of the stress path) as smooth as possible from point A to point B of the inclined notch. The standard deviation must be the smallest possible.

The nine figures on Table II-1 show the angle on the stress path in the p-q diagram depending on the position along the inclined notch (A-B). in every figure the angle of the stress path is depicted for two cases, which are the notch (1) and along the symmetry line of the shear surface (2). The values of 5, 7.5 and 10 mm are used for Y and 7, 7.5 and 10 mm for Z.

On that table the combination Y=7.5 and Z=7 [mm] delivers the best results. However the second combination Y=7.5 and Z=7.5 [mm] is chosen because the difference is negligible and shear failure is easier achieved due to higher shear forces. A study in Table II-2 confirms that the combination Y=7.5 and Z=7.5 [mm] is the best choice to optimize the geometry. It will be called geometry G1.

Table II-1: Evolution of the angle of the stress path in the p-q diagram depending on the position along the inclined notch (A-B) for 9 different combinations of the 60° inclined notch bar with the values of 5, 7.5 and 10 mm for Y and 7, 7.5 and 10 mm for Z.

Value of Y [mm]	7	7.5	10
10	$\bar{\alpha}$ =72.85 +/- 3.81° 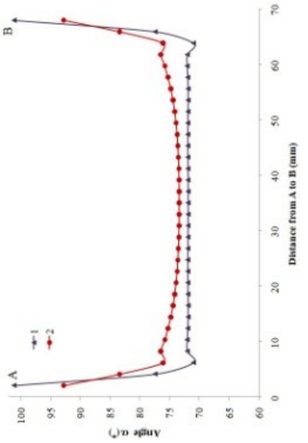	$\bar{\alpha}$ =72.96 +/- 3.89° 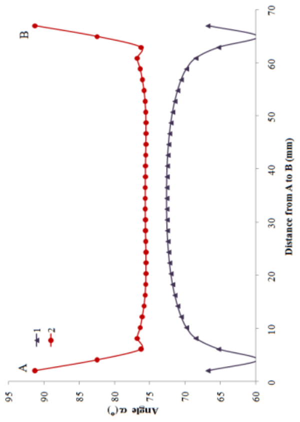	$\bar{\alpha}$ =73.53 +/- 4.18° 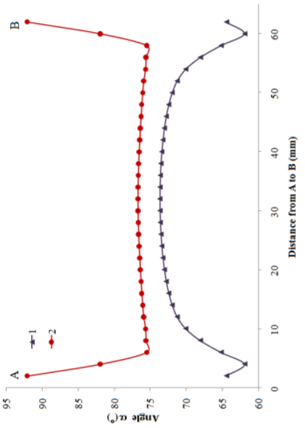
7.5	$\bar{\alpha}$ =72.92 +/- 3.43° 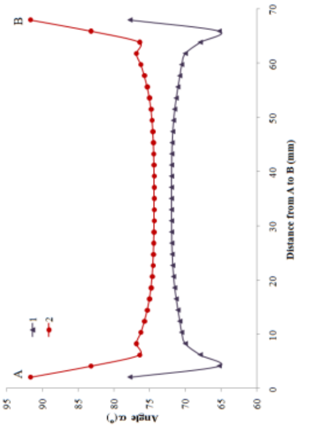	$\bar{\alpha}$ =72.99 +/- 3.44° 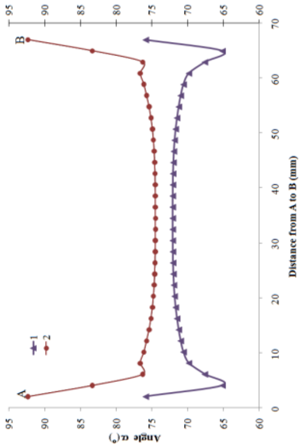	$\bar{\alpha}$ =73.48 +/- 3.69° 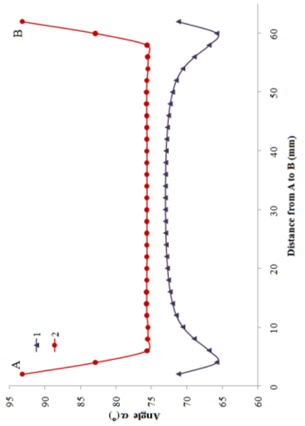
5	$\bar{\alpha}$ =73.94 +/- 5.38° 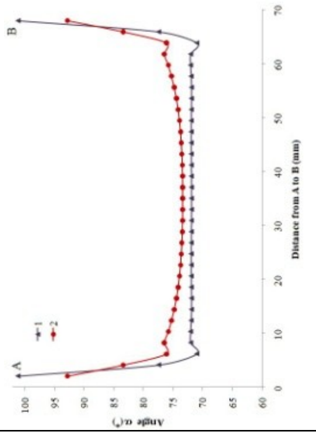	$\bar{\alpha}$ =73.98 +/- 5.17° 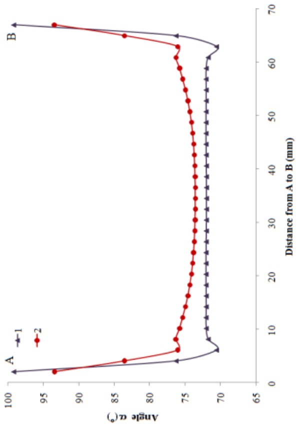	$\bar{\alpha}$ =72.85 +/- 4.56° 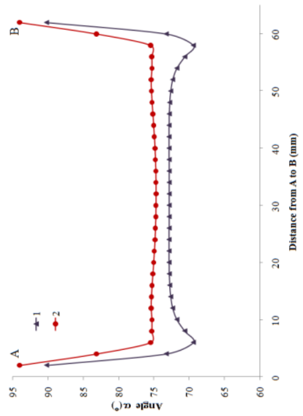

Value of Z [mm]

Table II-2: Mean angle of the stress path $\bar{\alpha}$ and standard deviation for 5 combinations of the 60° inclined notch bar with the values of 7, 7.5 and 8 mm for Y and Z. S is the shear area.

		Value of Y [mm]		
		7	7.5	8
Value of Z [mm]	7		**$\bar{\alpha}$=73.92° +/- 3.43°** S=1 572.85 mm^2	
	7.5	**$\bar{\alpha}$=73.14° +/- 3.54°** S=1 528.42 mm^2	**$\bar{\alpha}$=72.99° +/- 3.44°** S=1 505.92 mm^2	**$\bar{\alpha}$=72.91° +/- 3.46°** S=1 483.42 mm^2
	8		**$\bar{\alpha}$=73.08° +/- 3.48°** S=1 438.99 mm^2	

III.3.2 Notch thickness variation

The saw used to prepare the specimens is 3 mm thick. It was chosen to study the influence of the thickness of the notch on the geometry G1. Table II-3 shows the influence on the standard deviation of $\bar{\alpha}$. A decrease of thickness of the notch decreases significantly the $\bar{\alpha}$ and the standard deviation.

Table II-3: $\bar{\alpha}$ and standard deviation for two thickness of the notch.

Thickness of the notch	$\bar{\alpha}$ [°]	SD [°]
3 mm	72.99	3.44
2 mm	72.42	3.05

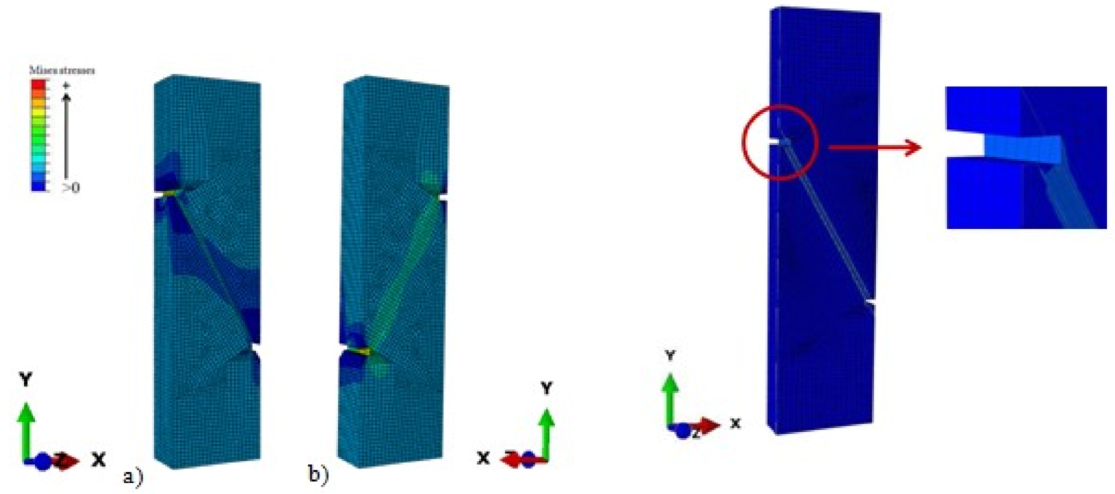

(i) (ii)

Figure II-16: (i) FEM model of a specimen with a 60° inclined notch and a notch of 3 mm.(a) front view, b) view of the symmetrical axis).(ii) FEM model of a specimen with a 60° inclined notch and a notch of 2 mm

The results obtained by combining two tests, i.e. a pure shear test and a combined loading compression-shear test with a 60° inclined notch geometry G1, would be interesting in the case that only pure shear failure occurs in the shear test. Some attempts were done for an inclined notch lower than 60° but no shear failure appeared. That is why a different geometry for a combined loading compression-shear test with an angle value higher than 60° will be used also.

III.4 80° double notched bar specimens

Another geometry with a different angle for the inclined notch is needed in order to achieve a different angle of the stress path. For an inclined notch higher than 80° buckling may occur. That is why 60° and 80° were chosen for the inclined notch since beyond these values for the inclination angle, the results are not exploitable.

The specimen geometry of the 80° double notched bar specimen has been optimized by finite element simulation. The aim is to obtain an α value (angle of the stress path) as smooth as possible from point A to point B of the inclined notch. Furthermore the standard deviation must be the smallest possible.

The combination Y=10 and Z=28 [mm] was chosen at the beginning of the study. This geometry will be called G2. A more thorough study for the optimization gives the best results for the combination Y=8.5 and Z=26 [mm]. A summary of the results is given in Table II-4. It can be concluded that the difference between the two combinations is negligible. So the laboratory results of the geometry G2 would be used also.

Table II-4: $\overline{\alpha}$ *and standard deviation for 2 different combinations of the 60° inclined notch bar. S is the shear area.*

Value of Z [mm]	Value of Y [mm]	
	8.5	10
26	**α= 76,334 +/- 3,02°** S=2 056.35 mm^2	
28		**α= 77,008 +/- 3,22°** S=1 685.42 mm^2

III.5 Uniaxial compression testing device

Since the uniaxial compression test can easily be used at elevated temperatures (Figures II-16 and II-17), the geometries G1 and G2 were designed taking into account the measures of the testing device. The test is carried out with a speed of 0.5 mm/min until rupture. A special experimental setup is necessary to a low horizontal movement of one end of the specimen. For this purpose, the specimen is situated on a horizontal plate, which rests on rolls. A ball joint between the axial piston and the upper plate guaranties an even contact with the upper plate and the top surface of the sample. For the remainder of the study, the maximum force will be used.

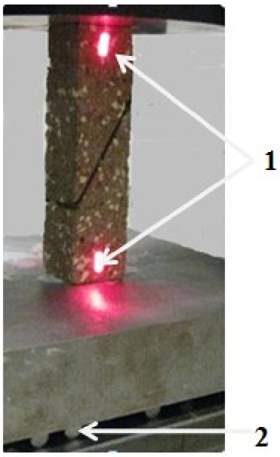

Figure II-17: Uniaxial compression test at room temperature. (1) laser speckle; (2) Rolls.

Figure II-18: Uniaxial compression test at elevated temperature.

III.6 Determination of the cohesion and friction angle

From p and q (Equations II-1 and II-2),

$$p = \frac{1}{3} \cdot (\sigma_1 + \sigma_2 + \sigma_3) \tag{II-1}$$

$$q = \sqrt{\sigma_1^2 + \sigma_2^2 + \sigma_3^2 - \sigma_1 \cdot \sigma_2 - \sigma_1 \cdot \sigma_3 - \sigma_2 \cdot \sigma_3} \tag{II-2}$$

the angle (α) in the p-q diagram of each element will be determined.

$$\alpha = \tan^{-1}\left(\frac{q}{-p}\right) \tag{II-3}$$

Figures II-21 and II-22 show the evolution of the angle of the stress path for G1 and G2. α is described along the inclined notch from A to B: (1) is situated parallel to the distance A-B in the symmetry plane of the specimen, (2) is situated on the surface of the inclined notch.

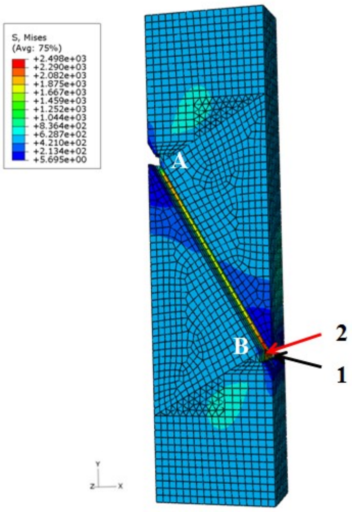

Figure II-19: FEM model for G1.

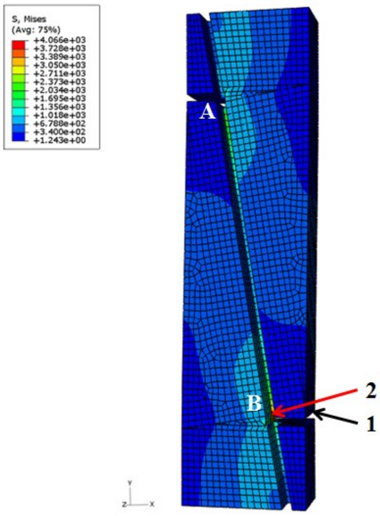

Figure II-20: FEM model for G2.

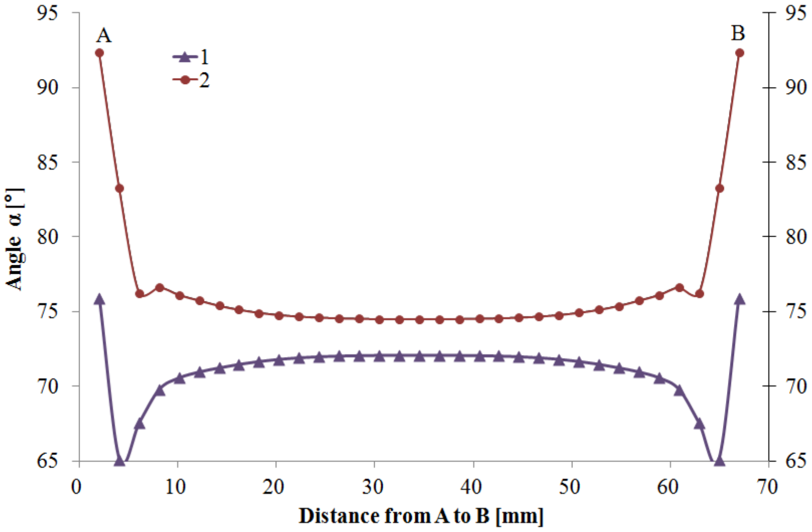

Figure II-21: Evolution of the stress path angle in the p-q diagram depending on the position along the inclined notch (A-B) for G1; (1) along the plane of symmetry, (2) along the notch root.

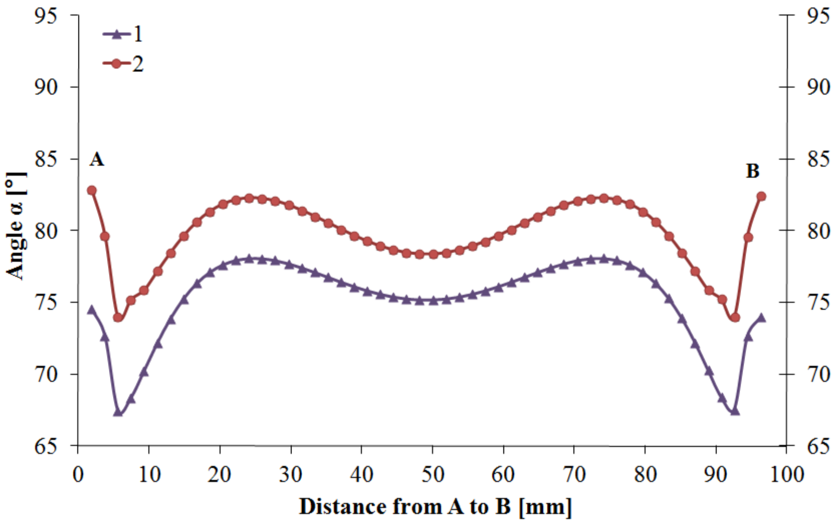

Figure II-22: Evolution of the stress path angle in the p-q diagram depending on the position along the inclined notch (A-B) for G2; (1) along the plane of symmetry, (2) along the notch root.

For both geometries, the mean $\bar{\alpha}$ was used for further evaluation.

Table II-5: Mean angle $\bar{\alpha}$ and standard deviation for G1 and G2.

Geometry	$\bar{\alpha}$ [°]	SD [°]
G1	72.99	3.44
G2	77.00	3.22

IV TORSION-COMPRESSION TEST: SAMPLE GEOMETRY OPTIMISATION WITH FEM

As seen in Table II-5, the difference of $\bar{\alpha}$ is rather small (4°) and quite low compared to the standard deviation expected for the tests performed. According to that a great number of tests would be necessary to assess a reliable value. To avoid this and simultaneously improve the reliability of the results, a new testing procedure will be applied.

A new designed specimen will be tested with torsion only and torsion-compression loading. The sample is a notched cylinder of 80 mm high and 40 mm in diameter. The notch depth and the ratio between torsion and compression are optimized by simulation. The machined notch enhances the probability of crack propagation in the ligament surface.

By simulation the principal stresses in the notch root have been calculated for a displacement of the upper specimen surface of -0.01 mm for the case of a Young's modulus of 20 GPa. These calculations have been performed for several torsions angles. From the results the angle of the stress path was calculated in dependence of the torsion angle.

This specimen type (G3) is drawn with the software ABAQUS CAE. The notched cylinder is 80 mm high and 40 mm in diameter. The notch is situated in the middle of the cylinder (see Figure II-23). The notch width was chosen to be 3 mm, the notch depth was varied between 1.5 and 4 mm. An axisymmetric model was used. The element type used is with 4 nodes (CGAX4). The meshed domain is uniformly distributed over the whole geometry. A finer mesh was used for the notch to divide it in three equal parts. As the Young's modulus choice does not affect the angle of the stress path, this parameter is fixed at 20 GPa and the Poisson's ratio to 0.3.

Several boundary conditions were used for this model. On the upper surface a vertical displacement of -0.01 mm along the y-axis was imposed, and different angles of axial rotation have been chosen. The bottom is locked in y direction and with respect of rotation. After linear elastic simulation, the calculation of α has been performed in the same way as for the modified shear test.

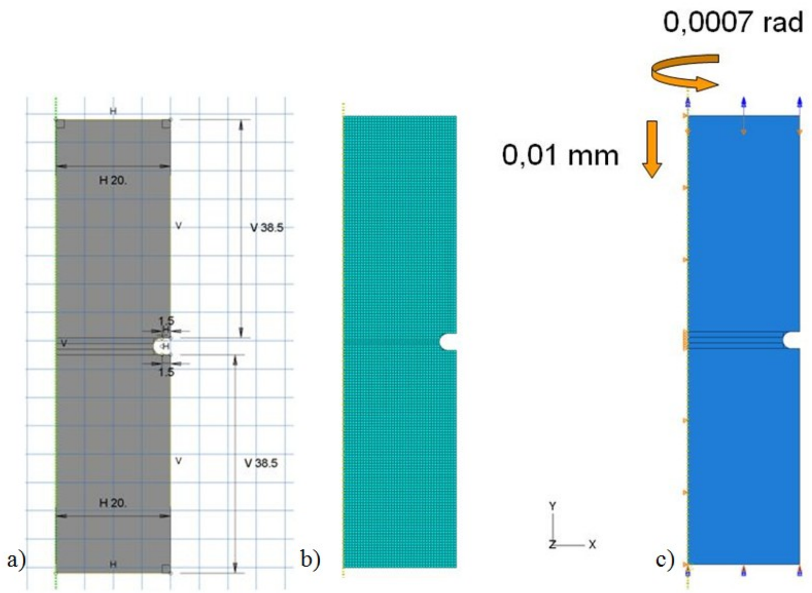

Figure II-23: Geometry G3, 3 mm notch depth. a) axisymmetric model, b) FEM model and c) boundary conditions.

To optimize the notch depth and the ratio between torsion and compression, simulations were done. Different notch depths were simulated, moreover for each notch depth the angle of rotation was changed until a minimum of the standard deviation of $\overline{\alpha}$ was found for the fracture surface while keeping the vertical displacement of -0.01 mm constant. Figure II-24 shows the stress path angle depending on the radius and the torsion angle for G3 with 3 mm notch depth. There is a higher influence of torsion angle close to the notch. If the sample is tested with pure torsion the angle of the stress path is 90° and the standard deviation is equal to zero.

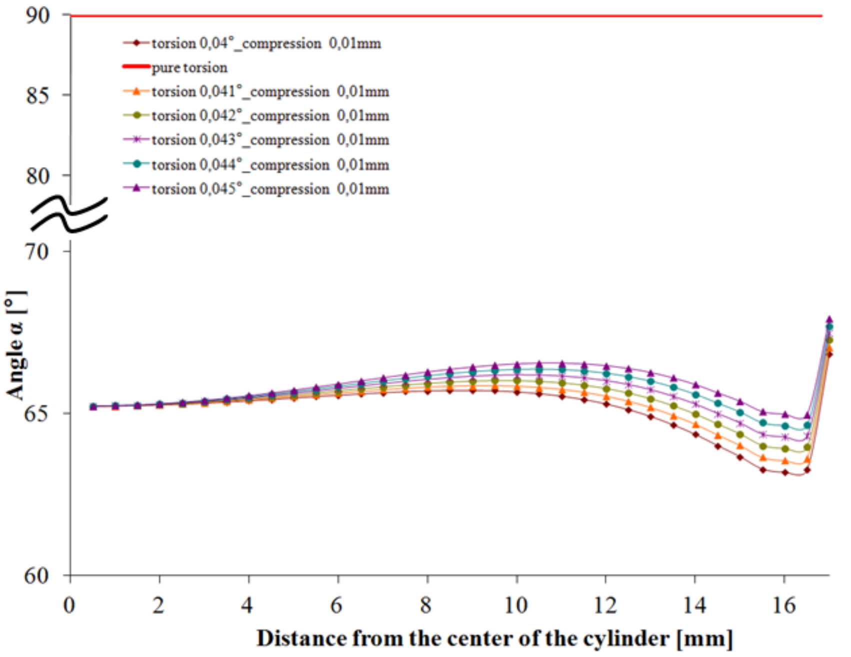

Figure II-24: Stress path angle in dependence of the radius and the torsion angle for G3 with 3 mm notch depth.

Figure II-25 shows the $\overline{\alpha}$ and the standard deviation in dependence of the torsion angle for G3 with 3 mm notch depth. The value of the $\overline{\alpha}$ increases while the torsion angle increases. The standard deviation reaches a minimum when the rotation is 0,044° with a compression of 0,01 mm. The values are summarized in Table II-7.

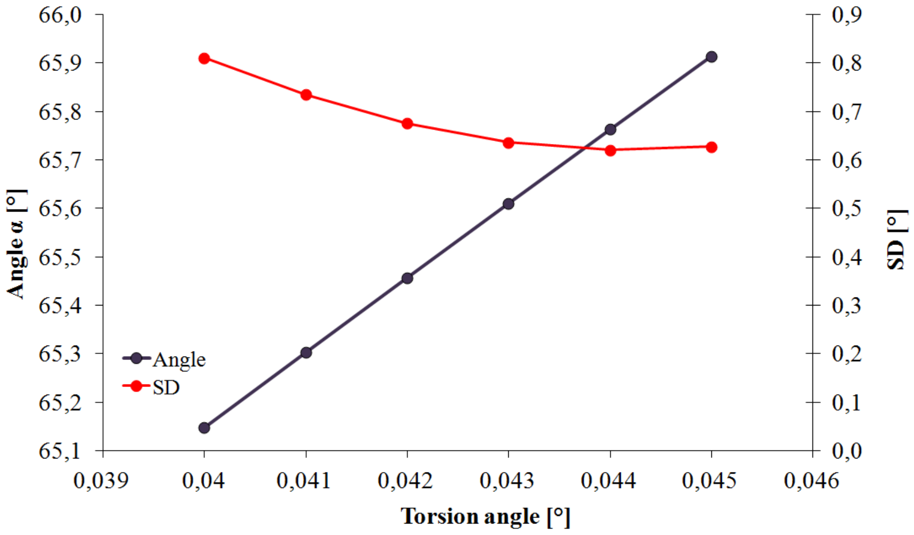

Figure II-25: $\overline{\alpha}$ and standard deviation depending on the rotation for G3 with 3 mm notch depth.

Table II-6: $\overline{\alpha}$ and standard deviation depending on the rotation angle for G3 with 3 mm notch depth.

Rotation [°]	Vertical displacement [mm]	$\overline{\alpha}$ [°]	SD [°]
0.04	0.01	65.15	0.81
0.041	0.01	65.3	0.73
0.042	0.01	65.46	0.67
0.043	0.01	65.6	0.64
0.044	0.01	65.76	0.62
0.045	0.01	65.91	0.63

Figure II-26 shows $\overline{\alpha}$ and the standard deviation in dependence of the notch depth for G3 with a notch depth from 1.5 to 4 mm. The chosen $\overline{\alpha}$ is the angle obtained with the rotation angle giving the lowest standard deviation for each notch depth. The value of $\overline{\alpha}$ decreases while the notch depth increases. Furthermore the curve of the standard deviation reaches a minimum for 3 mm notch depth.

Table II-7: Mean angle of stress path $\overline{\alpha}$ showing minimum standard deviation and associated standard deviation in dependence of notch depth for G3 for notch depth from 1,5 to 4 mm.

Depth of the notch (mm)	$\overline{\alpha}$ [°]	SD [°]
1.5	70.59	0.9
2	69.32	0.79
2.5	67.73	0.68
3	65.76	0.62
3.5	63.67	0.69
4	61.46	0.89

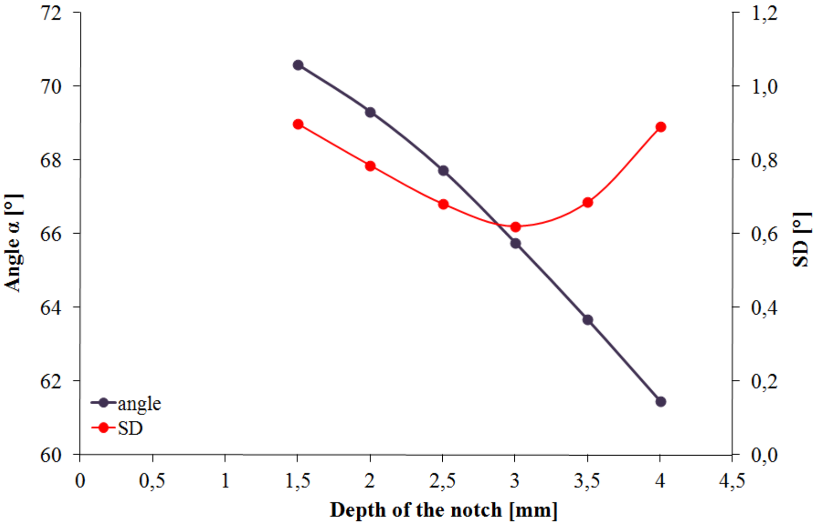

Figure II-26: Mean angle of stress path $\overline{\alpha}$ showing minimum standard deviation and associated standard deviation in dependence of notch depth for G3 for notch depth from 1,5 to 4 mm.

G3 with 3 mm notch depth will be used to determine the cohesion and the friction angle of refractory materials. The specimens will be tested by pure torsion (α=90° and SD=0°) and under torsion-compression while respecting the ratio between the rotation and the vertical displacement. The optimum result found was for a rotation of 0,044° and a vertical displacement of 0,01 mm i.e. a ratio of 0.227 between the vertical displacement and the rotation (α = 65,76° and SD = 0,62°).

V TRIAXIAL COMPRESSION TEST

The principle of a triaxial compression test is that the stress applied in the vertical direction (along the axis of the cylindrical sample) can be different from the stress applied in the horizontal directions perpendicular to the sides of the cylinder, i.e. the confining pressure. A homogeneous and isotropic material delivers a non-hydrostatic stress state, with shear stress that may lead to failure of the sample in shear.

V.1 Sample preparation

Several fifty millimeter diameter samples were core drilled. A length to diameter ratio of 2:1 was maintained. The two ends were ground flat and parallel in accordance with the ASTM guidelines for triaxial testing by a plan milling machine (Figure II-27). 3 samples for materials I and II were prepared. Samples were jacketed in polyolefin heat shrink tubing (Figure II-28) and sealed to the endcaps with twister copper wire. After applying the heat-shrink tubing, the chain of the gauge is wrapped around the sample and the two pins of the gage are set firmly against the jacket. Lateral expansion is measured with a circumferential gage. It measures the change in circumference directly and not the lateral expansion. It produces an “average” lateral strain value that is insensitive to local or directional variations in lateral strain. Another gage measures the axial displacement over a gage length of five centimeters (Figure II-29).

Figure II-27: Plan milling machine for producing specimens with parallel endfaces.

Figure II-28: Sample preparation. Heating the polyolefin tube on the sample to provide an impermeable barrier to confining pressure.

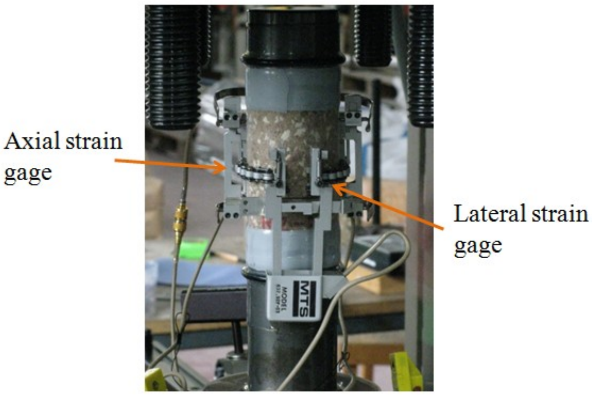

Figure II-29: Both lateral and axial extensometers mounted on the sample.

V.2 Multistage process

Tests were conducted with a servo-controlled hydraulic press **[PAGO-04]**. Two extensometers mounted on the sample measure the axial and the circumferential displacements. The test procedure is as follows:

First the confining pressure is increased to the first stage while the differential axial load is kept at a zero. A minimum load is applied to guarantee that the upper piston is in contact with the sample. At this point the displacement gages are zeroed and data acquisition initiates. Then the axial load is increased at constant confining pressure, axial and lateral strains are recorded whereas volumetric strain is calculated. All three strains are plotted continuously during the test. The loading is stopped when the sample shows signs of failure. The confining pressure was increased to the next level without removing the axial load. This procedure was repeated for as many confining pressures as required. It is possible to obtain several points in the p-q diagram. For each different confining pressure with its corresponding failure stress state, it is possible to draw a point in the p-q diagram (Figure II-30).

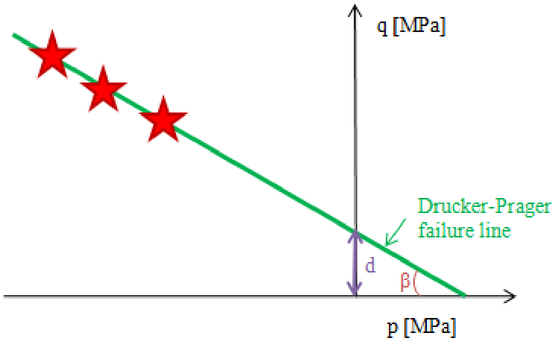

Figure II-30: Determination of Drucker-Prager failure line by a multistage triaxial test.

VI DOUBLE SHEAR TEST

The GEMH laboratory has introduced a double shear test to avoid the bending risk that can result from the direct shear test on a specimen **[BOUH-08, DIAK-07, DIAK-10]**. The test is used to investigate crack propagation within the two refractory materials. It is a symmetrized version of the direct shear test in terms of geometry and mechanical load. With a notched specimen, this test characterizes the shear behavior of material. Two lateral sides (Part 1 and Part 3) of the specimen are kept fixed throughout the test, the central part (Part 2) is subjected to monotonic loading. The interfaces of the specimen are tested in pure shear (Figure II-31).

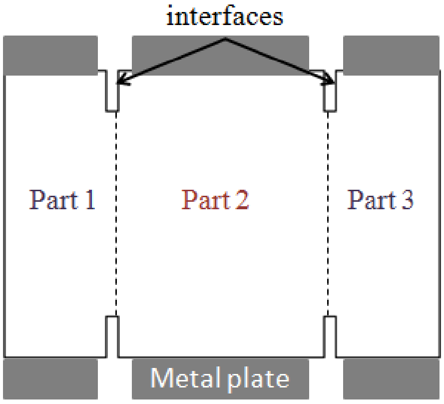

Figure II-31: Schematic diagram of the double shear test specimen.

VI.1 Sample preparation

3 samples of each refractory material were machined as shown on Figure II-32.

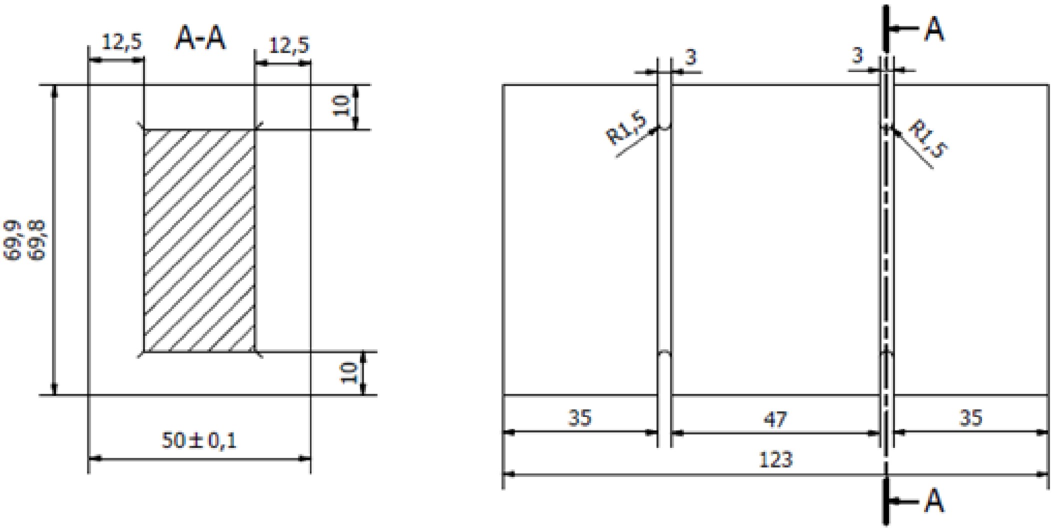

Figure II-32: Schematic drawing of the double shear test specimen.

To avoid bending stress at interfaces, steel plates are glued onto the bearing surfaces and loading surfaces of the specimen. Bonding is accomplished using a two-component adhesive. The polymerization of the glue is considered adequate after 4 hours. A device was used to glue steel plates (Figure II-33). This last step ensures the best alignment of steel plates in relation to the double shear loading configuration. Screws were used to fasten the plates glued onto the specimen with the DST device.

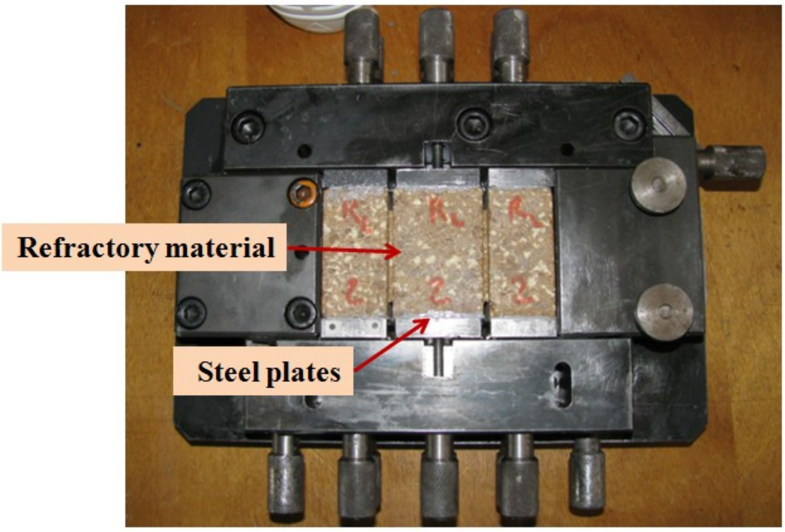

Figure II-33: Device for gluing metal plates onto specimen faces.

VI.2 Experimental configuration

A servo-hydraulic MTS® (Material Test System) press was used to apply the shear loading (Figure II-34). A load cell (+/- 100 kN) measures both the force values and relative tangential displacement values between the central part (Part 2) and the two lateral sides (Parts 1 and 3) of the specimen, using an external extensometer (+/- 1 mm). A LVDT sensor (Linear Variable Differential Transformer) (+/- 75 mm) measures the vertical displacement of the upper piston of the press. In determining the shear stress at the interface, it is assumed that both interfaces of the specimen are identical and behave the same way during the test (loading and tangential displacement).

The “average” nominal of the shear stress at the interface τ, i.e. the material cohesion, can be defined (Equation II-4) as the ratio between the measured loading F and the sum of the initial interface areas.

$$\tau = \frac{F}{S_L + S_R} \tag{II-4}$$

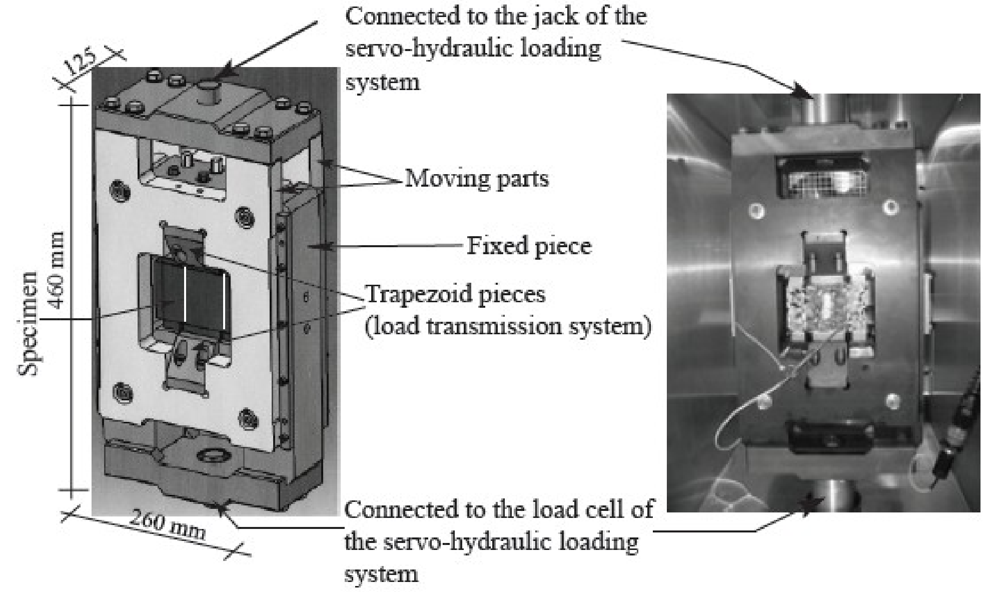

Figure II-34: Schematic presentation and photograph of the double shear test device.

VII MATERIALS CHOSEN TO VALIDATE THE DESIGN OF NEW SHEAR TESTS

To validate the new experimental tests, two different refractory materials have been chosen. The first is single phased as the matrix and the aggregates which compose the material have the same composition. The second one is a two-phase material composed of isotropic inclusions within an isotropic matrix in order to obtain a difference between the thermal expansion coefficients α of the phases. Indeed, a contraction of the matrix higher than those of the inclusions (Δα>0) subjects the matrix to circumferential tensile stresses and to radial compression in the cooling zone of the firing process. In this case the inclusion is in compression. When the matrix is not able to adjust to the deformation anymore, it can be expected that the exerted circumferential stress reaches a critical value and initiates radial microcracks (Figure II-35) **[HUGE-07, TESS-03]**.

As the mechanical behavior of these two kinds of materials is different, it can be expected that the evolution of the behavior of the Drucker-Prager parameters will be different in dependence of temperature. The two tested materials are manufactured by RHI AG.

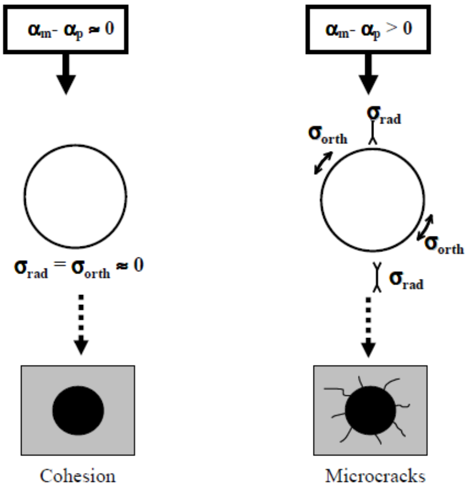

Figure II-35: Internal stresses involved by thermal expansion mismatch between phases ***[TESS-03]****.*

VII.1 Microstructure analysis

An optical observation of material I shows that this product is composed of aggregates, inferior to 4 mm, in a magnesia matrix (Figure II-36).

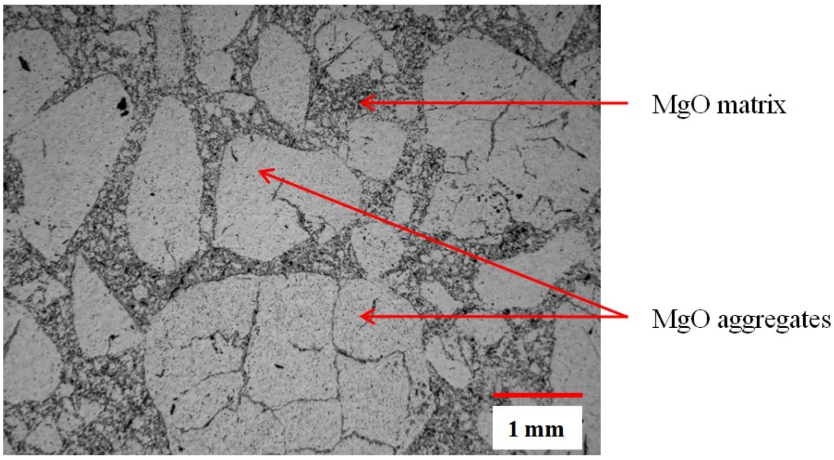

Figure II-36: Microstructure of material I as observed by reflected light microscopical investigation.

Pure magnesia products, like material I, are e.g. used in regenerator checkerwork and walls. This magnesia brick is characterized by low iron and fluxing agent contents, leading to high refractoriness under load. The composition reveals a majority of magnesia (MgO) with significant amount of lime (CaO) and silicate (SiO_2). Concerning the crystalline phases composition obtained by X Ray Diffraction (XRD), the predominant detected phase is Periclase (MgO).

Table II-8: Chemical composition of materials I and II; data provided by the manufacturer RHI AG.

	MgO	Al_2O_3	Fe_2O_3	CaO	SiO_2	Density	Porosity
Material I	97%		0.5%	1.6%	0.6%	3.01 g/cm^3	19.0 vol%
Material II	87.5%	10.5%	0.6%	1.0%	0.4%	3.01 g/cm^3	15.0 vol%

Optical observation of material II (Figure II-37) shows that it is composed of MA spinel aggregates ($MgAl_2O_4$) with a grain size of 3 to 5 mm, and magnesia aggregates (MgO) with 0.2 to 4 mm grain size, magnesia fines with a grain size below 200 µm from the matrix. The chemical composition of this material is resumed in Table II-9.

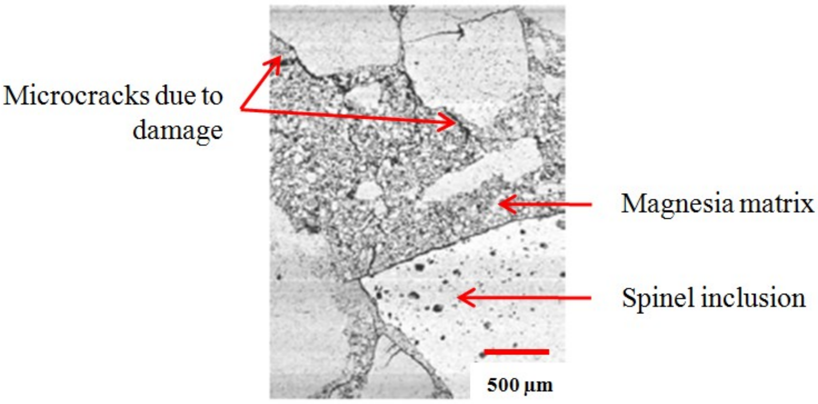

Figure II-37: Microstructure of material II as observed by reflected light microscopical investigation..

Burnt magnesia spinel bricks like material II are used in cement rotary kiln linings. The thermal expansion mismatch between the magnesia matrix ($\alpha \approx 13 \cdot 10^{-6}$ K^{-1}) and the spinel inclusion ($\alpha \approx 9 \cdot 10^{-6}$ K^{-1}) is responsible for radial microcracks around the spinel inclusions which appeared during the cooling stage of manufacturing process. This type of brick shows high flexibility, excellent thermal-shock resistance, excellent resistance to chemical attack and a high refractoriness.

VII.2 Elastic properties

Figure II-38a shows a nearly linear dependence of the Young's modulus from the temperature. The decrease of the Young's modulus observed during heating is only due to the decrease of interatomic potential i.e. the weakening of chemical bonds (opposite situation during the cooling). The Young's modulus measured with RFDA **[DAHL-09, ROEB-02**] at room temperature in flexion is 105.5 GPa (+/- 3.98 GPa), while the Young's modulus of a 100%-dense magnesia product is about 300 GPa. Young's modulus decrease is due to pores and flaws; especially flaws largely deviating from spherical shape have a great influence on Young's modulus.

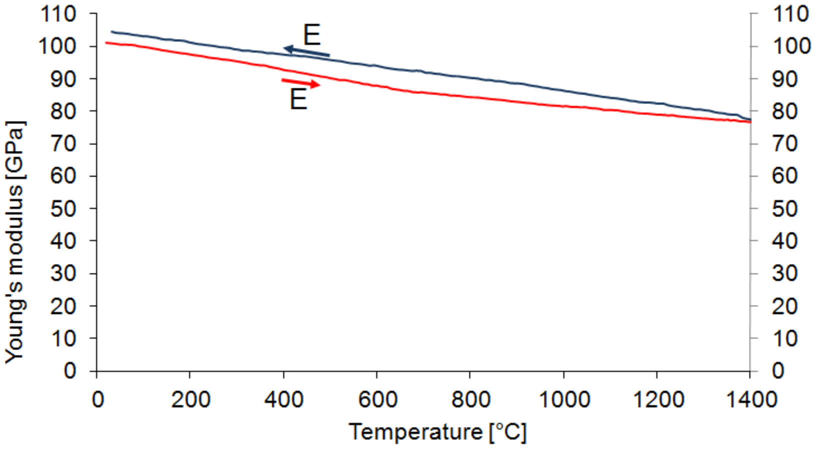

-a-

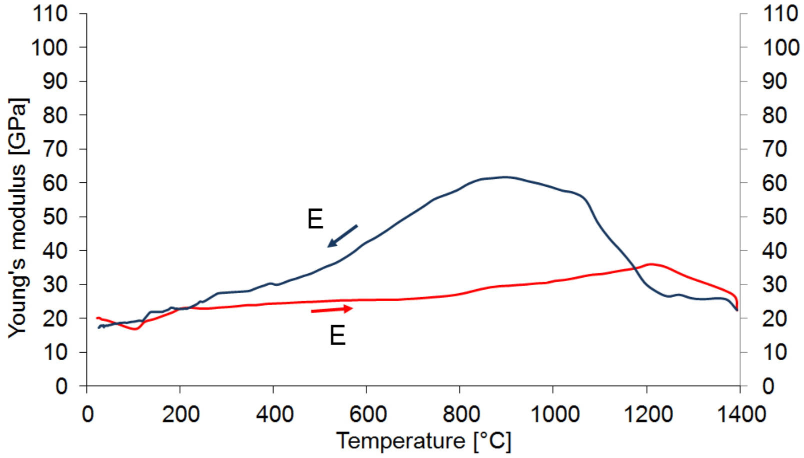

-b-

Figure II-38: Young's modulus evolution in dependence of temperature from room temperature up to 1400°C of (a) material I and (b) material II.

As material II contains microcracks a hysteresis of the Young's modulus temperature curve was expected. The result is shown in Figure II-38b. From room temperature to 1200°C the Young's modulus increases because of the microcracks closing. The heating part of the Young's modulus-temperature curve has a maximum at 1250°C and the maximum of the cooling part is reached at 900°C. Furthermore, the maximum of the Young's modulus in the heating part is lower than the maximum in the cooling part of the curve. From 1000°C, the Young's modulus decreases due to the reopening of existing microcracks in the matrix or creation of new ones. The Young's modulus measured with RFDA at room temperature in flexion is 7,1 GPa (+/- 0,85 GPa). The high amount of microcracks can explain the small Young's modulus.

VII.3 Work of fracture

The wedge splitting test is a mechanical destructive test designed foe the determination of the specific fracture energy **[TSCH-86]**. Specific fracture energy is determined from load/displacement diagram.

Figure II-39 presents, for the two studied materials, the horizontal force in dependence of the horizontal deformation obtained during wedge splitting tests. Fracture energies of material I and material II are 135 N.m^{-1} and 170 N.m^{-1}, respectively.

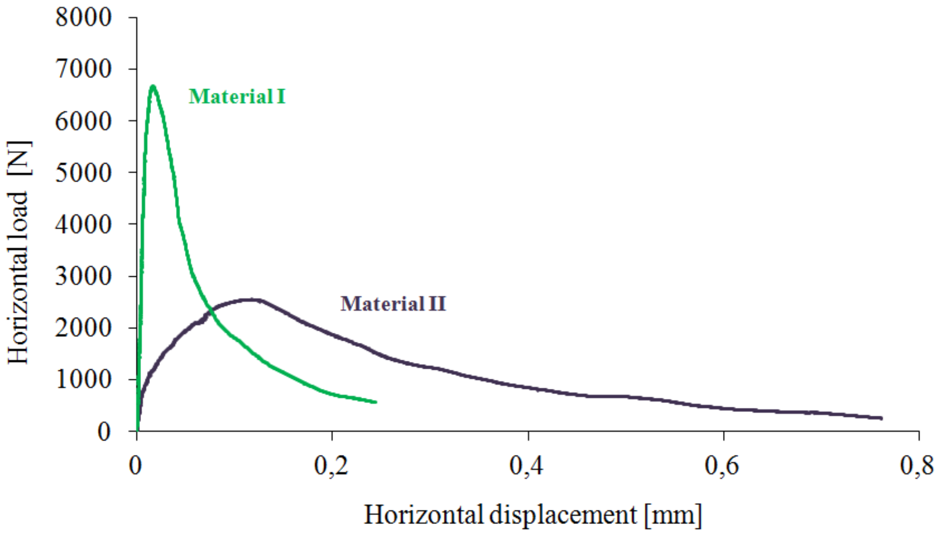

Figure II-39: Load-displacement curves obtained from the wedge splitting test.

Material I shows a by far higher maximum load and a lower ultimate horizontal displacement compared with material II. This is characteristic for a more little behavior of material I. the brittleness decrease of material II is achieved by a lower strength and a somewhat higher specific fracture energy. Both may be contributed to the existence of prefabricated microcracks. On the one hand they decrease the strength, on the other hand they may give rise to crack branching and by this increase fracture energy.

VIII CONCLUSION

A part of this work was devoted to the development of a new experimental method to determine the Drucker-Prager parameters at elevated temperatures. The modified shear test and the torsion/compression test can determine the cohesion and the friction angle of materials at elevated temperatures. Both have been optimized by FEM simulations.

The multistage triaxial test, the pure torsion test and the double shear test can be implemented at room temperature; refractory materials will be tested to compare them with the modified shear test and the torsion/compression test.

This chapter described the two refractory materials chosen to validate the design of new shear tests. Due to their large differences in microstructure, strength, Young’s modulus and brittleness also different values for cohesion and friction angle in dependence of temperature might be expected.

CHAPTER 3:

EXPERIMENTAL RESULTS

I INTRODUCTION

The two refractory materials have been tested by modified shear test, multistage triaxial test, double shear test and by torsion and torsion/compression tests at room temperature. The results obtained will be compared and discussed. Moreover the modified shear test also has been performed at elevated temperatures. The multistage triaxial test will be used to validate the modified shear test and the torsion/compression test at room temperature. Moreover the torsion test and the double shear test enable a comparison of the cohesion at room temperature with the results of the modified shear test and the torsion compression test.

II LABORATORY RESULTS AT ROOM TEMPERATURE

II.1 Modified shear test

II.1.1 Evaluation of Drucker-Prager parameters

At room temperature, G1 and G2 are tested with a uniaxial compression testing device. A typical result (material I with geometry G2) can be observed on Figure III-I. Material failure is obtained suddenly when the maximum force (approximately 30,4 kN) is reached. The results of materials I and II are summarized in Table III-1. For materials I and II, 3 samples are tested for each geometry.

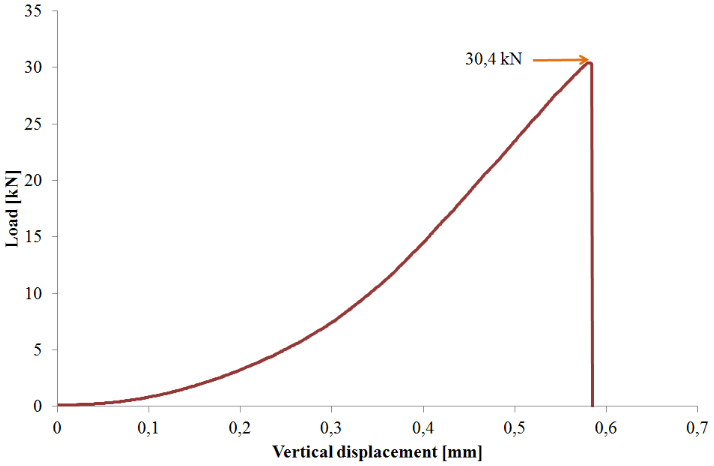

Figure III-1: Load-displacement diagram for material I with geometry G2.

Table III-1: Results for materials I and II.

		Maximum load [kN] (G1: 60°)	Maximum load [kN] (G2: 80°)
Material I	Average	48.4	31
	SD	0.2	0.97
Material II	Average	36.1	10.9
	SD	0.6	0.8

The principal stresses have been determined under experimental conditions from those of the linear elastic simulation by dividing the simulation results by the load used for simulation and multiplying then with the load measured from the experiment. Then the invariants have been calculated (Table III-2).

Table III-2: The coordinates p and q for the materials I and II and the geometries G1 and G2.

	Geometry G1		Geometry G2	
	p [MPa]	q [MPa]	p [MPa]	q [MPa]
Material I	-15.5	50.5	-10.1	42.5
Material II	-11.6	37.8	-3.6	14.9

Then the cohesion (d) and the friction angle (β) are calculated from the coordinates p_{G1} and q_{G1} for G1 (point 1) and p_{G2} and q_{G2} for G2 (point 2) (III-1 and III-2).

$$d = q_{G2} - p_{G2} \cdot \frac{q_{G2} - q_{G1}}{p_{G2} - p_{G1}} \tag{III-1}$$

$$\beta = \tan^{-1}\left(\frac{q_{G2} - q_{G1}}{p_{G1} - p_{G2}}\right) \tag{III-2}$$

Figures III-2 and III-3 illustrate respectively the results of the Drucker-Prager parameters of material I and material II. Material I has a cohesion of 28.6 MPa and a friction angle of 54.8°. While the cohesion of material II is 5.2 MPa and the friction angle 70.4°. This means both materials show a clear difference with respect to failure under combined compressive and shear loads.

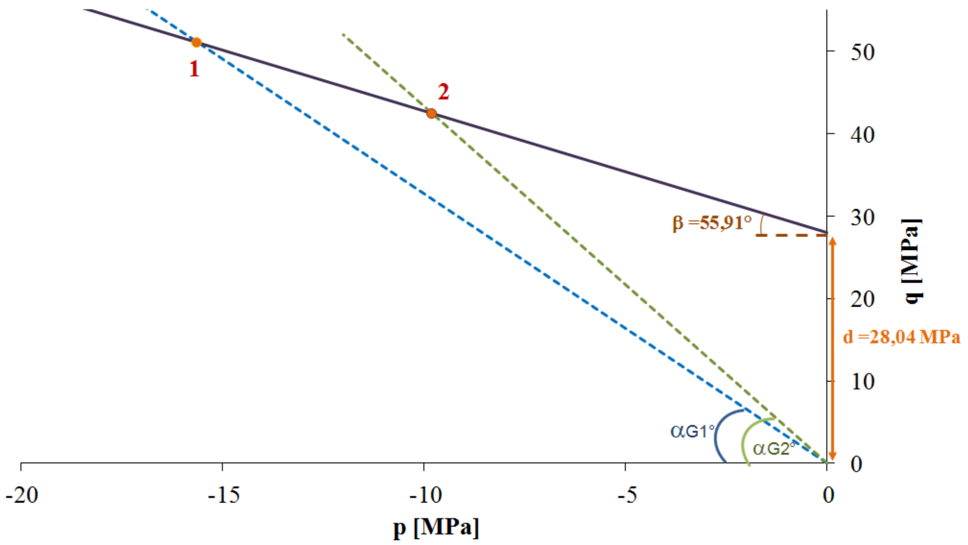

Figure III-2: Evaluation of cohesion d and friction angle β at room temperature for material I.

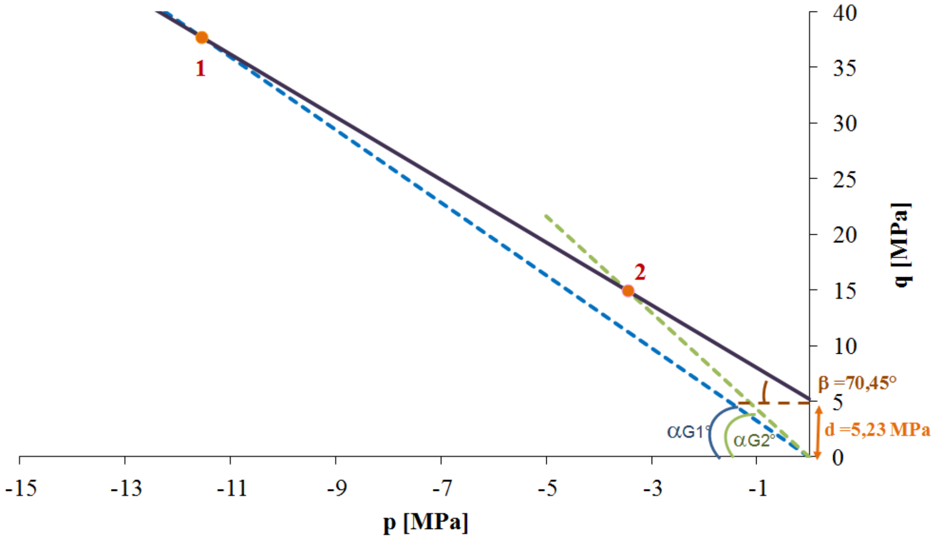

Figure III-3: Evaluation of cohesion d and friction angle β at room temperature for material II.

II.1.2 Evaluation of the Mohr-Coulomb parameters

As describe in chapter II, σ_1, σ_2 and σ_3, are directly calculated from the simulated geometries. The friction angle and the cohesion can be determined in the p-q diagram while considering the three dimensional stress state. Changes in the inclination of the notch have a small influence of the stress path in the p-q diagram. Due to the fact that q is a scalar there is no information about the direction of the corresponding shear stress.

It is also interesting to perform the evaluation with the help of Mohr's circle (Figure III-4). The vertical load leads to the minimum principal stress σ_3, this stress is assumed to be in the same direction as the load and both the middle and the maximum principle stresses are zero in the ligament area. σ_3 is calculated as the ratio between the maximum load and the projected shear area (Figure III-5 and equation III-3).

$$\sigma_3 = \frac{F_{v\,max}}{A_{proj}} \tag{III-3}$$

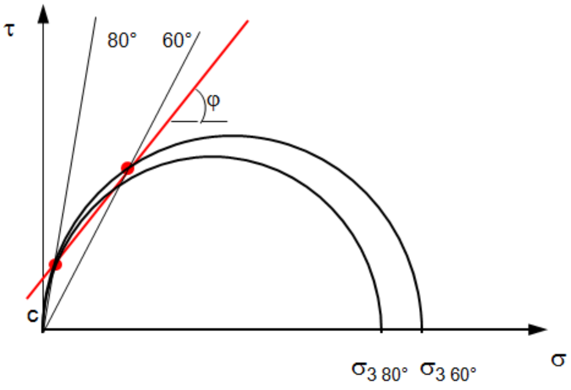

Figure III-4: Evaluation applying Mohr's circle.

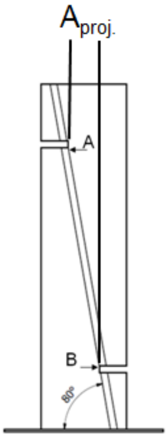

Figure III-5: Shear area projection.

The evaluation with the Mohr's Circles has been done for all samples. Figure III-6 illustrates the comparison between evaluation types, i.e. the evaluation made directly with the Mohr's Circles, the evaluation made from the simulation of the geometries and experimental tests, and the evaluation from multistage triaxial test. The multistage triaxial test is used to determine the cohesion and friction angle with the Mohr's Circles. It can be seen that the evaluation from the simulation and the evaluation from multistage triaxial test fit well. However the evaluation made with the Mohr's Circles is far from the multistage triaxial test results. This difference is due because the minimal principal stress is not in the same direction that the vertical load and the maximum principal stress is not zero (Figure III-7). It has to be taken into account that the middle principle stress is neglected in the σ-τ diagram. This implies an error up to 30% in strength **[HE-10]**. Furthermore, stress concentrations due to the notch effect have not been taken into account by the evaluation with the Mohr's Circle. Therefore the evaluation with the Mohr's Circles will not be use for the study.

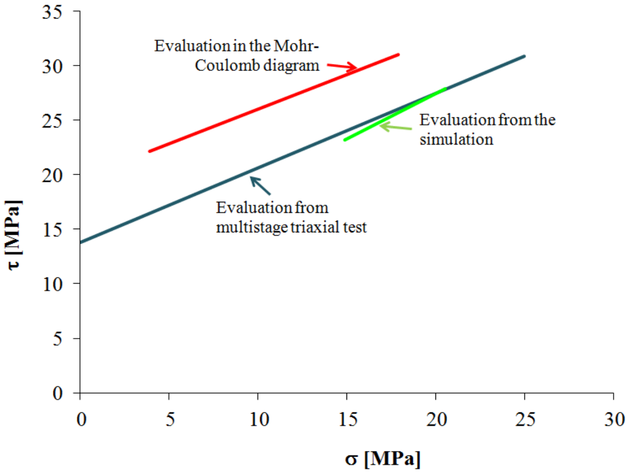

Figure III-6: Comparision of evaluation with the Mohr's Circles, evaluation from the simulation and evaluation from multistage triaxial test.

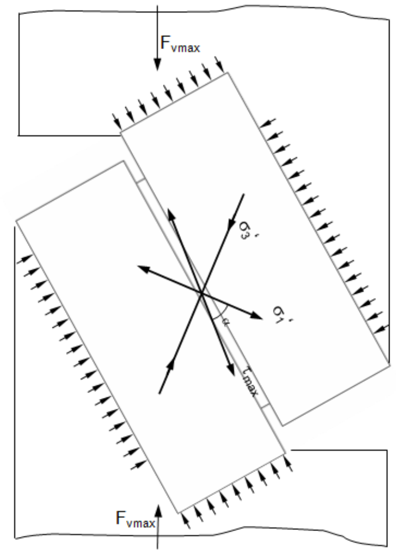

Figure III-7: Localisation of principal stresses and load in the modified shear test.

II.2 Multistage triaxial test

To validate the results of the modified shear test, multistage triaxial tests are conducted. The multistage triaxial test results are illustrated in the Mohr-Coulomb diagram. Figure III-8 shows a typical representation of Mohr circles and failure envelope obtained from multistage triaxial test of material I. To compare the results obtained with triaxial test with the modified shear test, the results were converted in the p-q diagram; a summary is on Table III-3. A scatter of the Drucker-Prager parameters can be observed. That may be due to the inhomogeneity of the materials. It has to be taken into account that the middle principal stress is neglected in the σ-τ diagram.

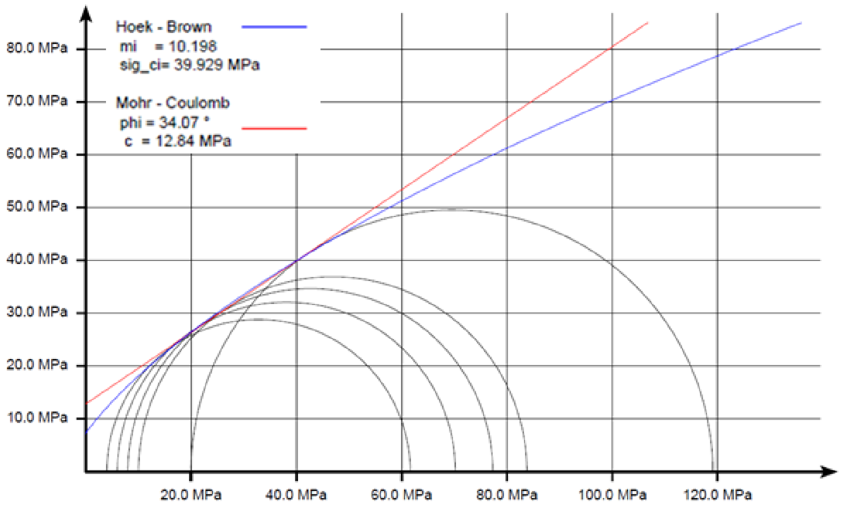

Figure III-8: Mohr circles representation and failure envelope obtained from multistage triaxial test of material I.

Table III-3: Mohr-Coulomb and Drucker-Prager parameters results obtained with the multistage triaxial test for material I and II.

		Mohr-Coulomb		Drucker-Prager	
	Sample number	φ [°]	c [MPa]	β [°]	d [MPa]
Material I	1	34.1	12.8	53.6	27.1
	2	37.3	9.67	53.5	24.1
	3	34.3	13.8	54.9	26.5
Material II	1	40.4	12.4	65.9	10.1
	2	39.9	12.4	60.2	20.1
	3	40.1	11.4	61.9	16.3

Figures III-9 and III-10 show the results of multistage triaxial tests and of the modified shear test for each material. The results are comparable to those obtained with the modified shear tests.

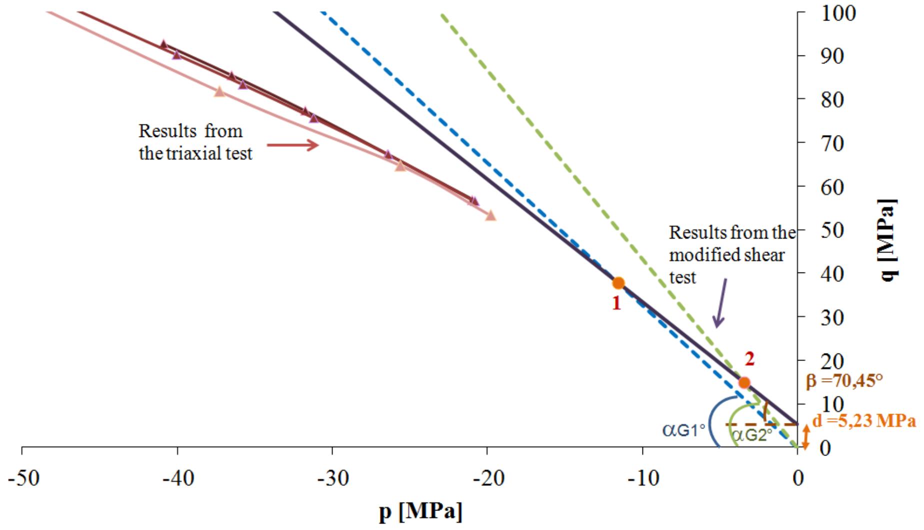

Figure III-9: Comparison of multistage triaxial test results with results from the modified shear test for material I.

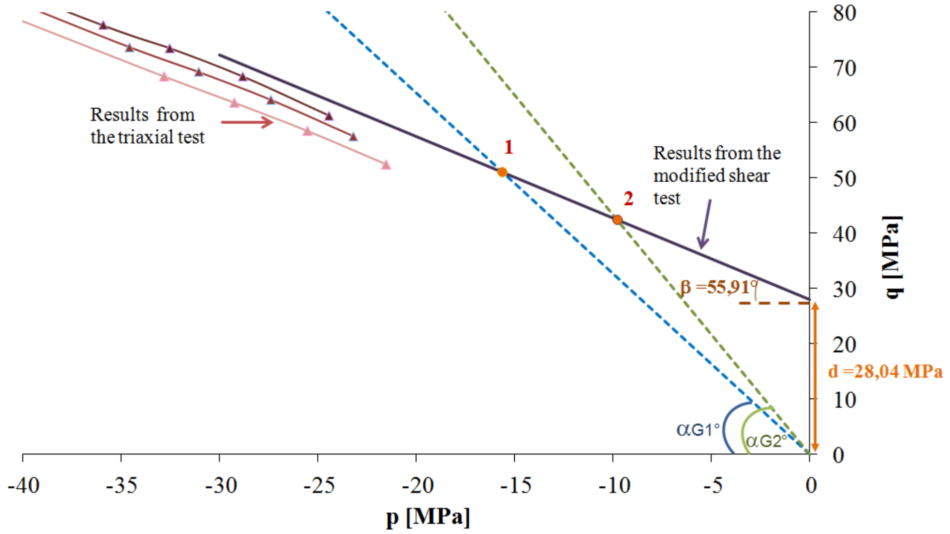

Figure III-10: Comparison of multistage triaxial test results with results from the modified shear test for material II.

II.3 Double shear test

The materials are tested with the double shear test in the GEMH laboratory in order to determine the cohesion. For each test, the force and displacement are measured, allowing the characterization of a shear stress/displacement curve. The cohesion can be defined as the ratio between the maximum measured shear stress and the sum of the initial sections of the specimen interfaces.

The cohesion of material I is 12.6 MPa and that of material II is 12.8 MPa. The results do not show the same difference between the materials as the other testing methods used. These tests results therefore do not seem to be reliable. As a consequence they will not be taken into account to evaluate the cohesion.

II.4 Torsion-compression test

Pure torsion tests are performed with optimized samples. At room temperature, G3 specimen is tested with a loading rate of 0.06°/s. Cohesion values of 27.0 MPa and 7.6 MPa are respectively found for material I and material II. These results are in total agreement with the preceding tests, i.e. the modified shear test results and the multistage triaxial test results.

In addition, torsion/compression tests are also carried out only at room temperature (For the two materials, 4 samples in each case are tested). For each experimental result, a FEM simulation is performed with the maximum torsion angle and the corresponding load in order to determine the coordinates in the p-q space. The load and the torsion moment occurring at the moment of torsion failure have been used for further evaluation. Only the first four elements from the surface of the ligament area (which represents 2 mm) are used for the evaluation. The results are summarized on Table III-4. In order to evaluate the Drucker-Prager parameters from these results, they have to be combined with those of another testing method.

Table III-4: Invariants p and q for materials I and II and the Geometry G3.

	p [MPa]	q [MPa]
Material I	-34.25	84.60
Material II	-23.72	64.61

II.5 Comparison and discussion of the results

In order to validate the modified shear test and the torsion/compression test, it is necessary to compare the three different methods: pure torsion test, torsion/compression test and the two modified shear tests.

Figures III-11 and III-12 illustrate the Drucker-Prager failure line obtained with the three different methods for material I and material II, respectively. There is a good correlation between the above mentioned methods. Material I has a cohesion of 26.1 MPa and a friction angle of 59.3°, the cohesion of material II is 7.6 MPa and its friction angle 67.7°. So the modified shear test and the torsion/compression test can be validated by their agreement with each other. These testing methods can be used for the evaluation of the evolution of the Drucker-Prager parameters in dependence on temperature. As the necessary equipment for the torsion/compression test was not available for elevated temperatures, only the modified shear test will be used at elevated temperature.

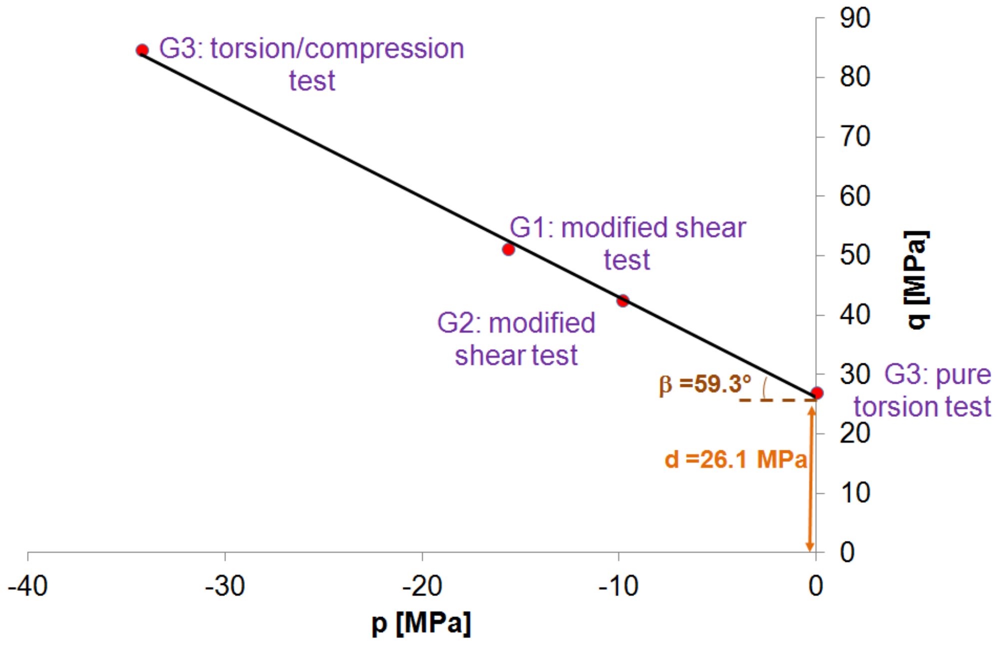

Figure III-11: Evaluation of Drucker-Prager parameters obtained at room temperature with the 3 methods for material I.

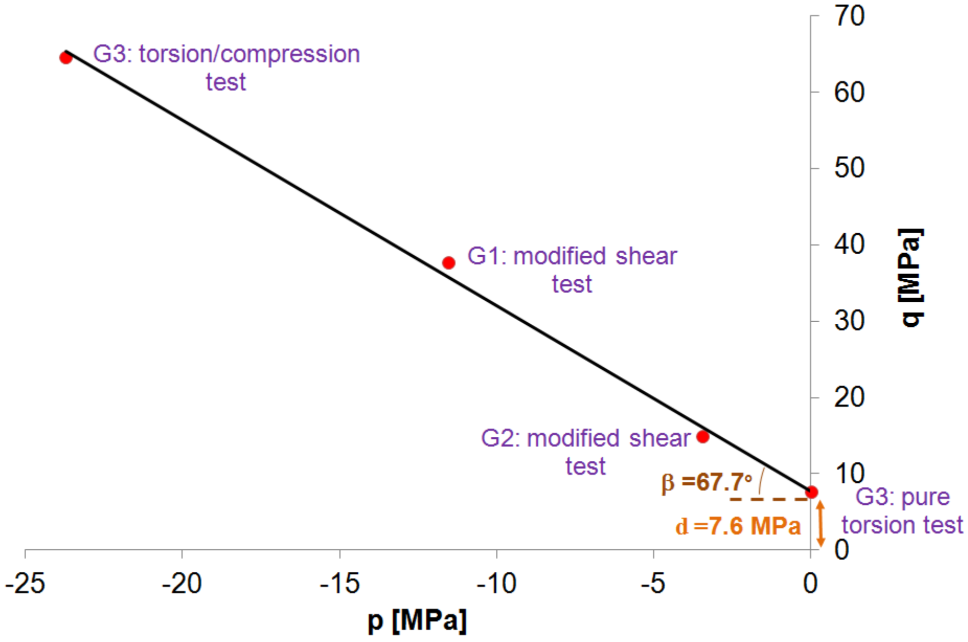

Figure III-12: Evaluation of Drucker-Prager parameters obtained at room temperature with the 3 methods for material II.

III LABORATORY RESULTS AT ELEVATED TEMPERATURE

The study of the Drucker-Prager parameters at elevated temperature is performed with the modified shear test. Specimens are tested with a uniaxial compression testing device including a furnace at 900, 1200 and 1400°C. The results are summarized on Table III-5. 3 samples are tested for each geometry and each temperature.

Table III-5: Friction angle and cohesion of materials I and II at 900, 1200 and 1400°C.

	900°C		1200°C		1400°C	
	β [°]	d [MPa]	β [°]	d [MPa]	β [°]	d [MPa]
Material I	62	15.6	65.7	12.5	67.9	10.0
Material II	69.7	7.7	68.8	6.0	69.6	0.7

Figure III-13 and Figure III-14 illustrate the evolution of the friction angle and cohesion from room temperature up to 1400°C including measurement errors. When comparing the evolution of the cohesion with the evolution of the Young's modulus (Figure II-38a for material I and Figure II-38b for material II), it is noticed that the evolution of the cohesion and the Young's modulus for the two materials shows a similar tendency from room temperature up to 1400°C. For material I, this can be explained by the softening behavior at elevated temperatures. For material II, Young's modulus and cohesion (strength) both seem to depend on the evolution of the microcrack network with temperature. The friction angle of material I increases when the temperature rises. To the contrary, the friction angle of material II is nearly independent from temperature.

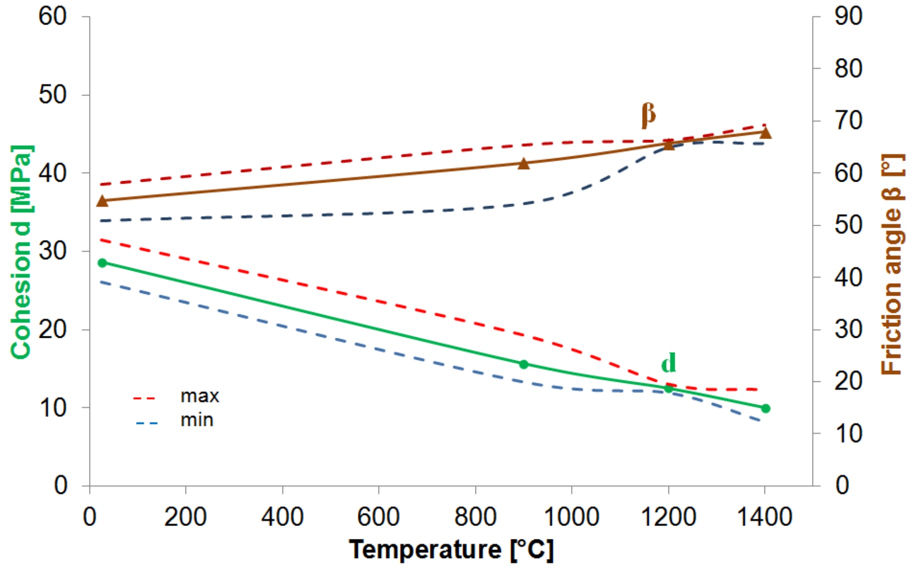

Figure III-13: Evolution of the friction angle and the cohesion of material I from room temperature up to 1400°C.

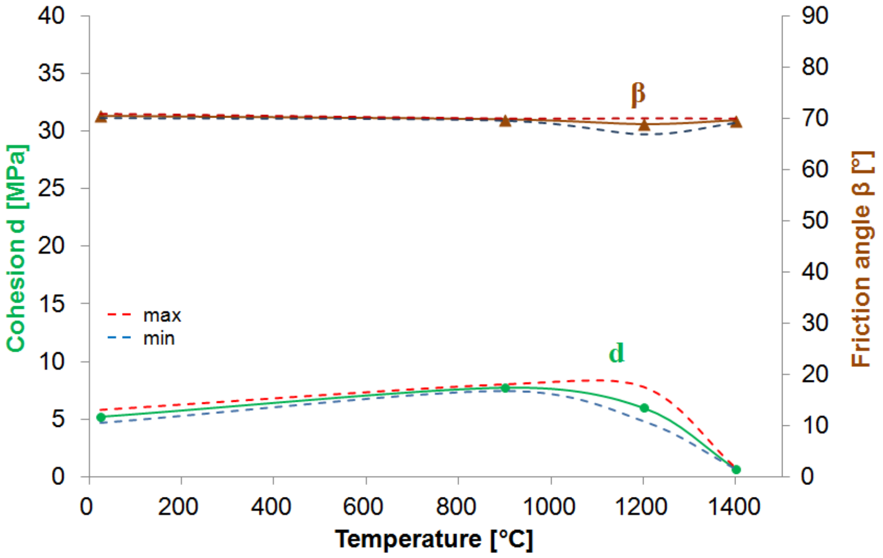

Figure III-14: Evolution of the friction angle and the cohesion of material II from room temperature up to 1400°C.

IV CONCLUSION

The modified shear test has been validated by comparing the results with those obtained by multistage triaxial tests. The multistage triaxial test is commonly used to determine the cohesion and friction angle of materials at room temperature. Satisfying correlation between the results was observed: by comparing the results obtained through modified shear test, torsion test and torsion/compression test, all these methods fit well. As a conclusion, the cohesion and the friction angle can be determined by combining these methods at room temperature and at elevated temperature.

CONCLUSION AND FUTURE PROSPECTS

For two refractory materials cohesion a friction angle have been determined at room temperature and elevated temperatures. It has been observed that the cohesion shows a temperature dependence which is related to that of Young's modulus and strength. In case of magnesia-spinel materials it is therefore also linked to closing of micro cracks during heating. The temperature dependence of the friction angle is so far not understood.

At room temperature agreement of torsion/compression results with other testing methods has been observed. This opens the possibility to apply this method at elevated temperature. This specimen shape may rather easily be tested heated up in a suitable furnace, too. A further investigation to be done in future would be the application of an inverse FEM evaluation of the modified shear test and the torsion/compression test. As the principle stresses and the invariants calculated from them are not constant on the whole shear surface – an average has been used for the modified shear test – this evaluation procedure might help to increase reliability and accuracy of the testing method.

The multistage triaxial test has been used in order to validate the modified shear test. The multistage triaxial test has been adopted as an alternative to a series of single-stage triaxial tests to determine engineering material parameters. It has been demonstrated that in some cases a difference can be observed between the two methods **[KIM-79]**. So far it has not been investigated whether single and multistage triaxial test yield similar results for refractory materials. That is why, in the future, the comparison between the results of single stage and multistage triaxial tests would be interesting.

Moreover within the investigations performed the unsatisfying behavior of the double shear test could not be explained. Obviously this method is very sensitive to undesired loading perpendicular to the shear surface, and it should be investigated whether this might occur or not. Also this would be an objective for further investigations.

REFERENCES

[ANDR-03] Andreev, K., Harmuth, H.: FEM Simulation of the thermo-mechanical behavior and failure of refractories – a case study. *Journal of Materials Processing Technology*, 143-144, 72-77 (2003).

[BAHL-09] Bahloul, O.: Evolutions en fonction de la température de propriétés élastiques de bétons réfractaires à base de carbure de silicium. Ph.D., *Université de Limoges (2009).*

[BENZ-08] Benz, T., Schwab, R., Kauther, R.A., Vermeer, P.A.: A Hoek-Brown criterion with intrinsic material strength factorization. *International Journal of Rock Mechanics & Mining Sciences*, 45, 210-222 (2008).

[BOUH-08] Bouhas, F., Millien, A., Pop, O., Petit, C.: Apport de la corrélation d'images à l'étude du comportement des enrobés bitumineux en fatigue par cisaillement. *XXVI^e Rencontres Universitaires de Génie Civil, Nancy*, 4 au 6 juin 2008.

[BOTE-07] Botelho, E.C., Pardini, L.C., Rezende, M.C.: Evaluation of hygrothermal effects on the shear properties of Carall composites. *Materials Science and Engineering*, A, 292-301 (2007).

[CLAU-08] Clausen, J., Damkilde, L.: An exact implementation of the Hoek-Brown criterion for elasto-plastic finite element calculations. *International Journal of Rock Mechanics & Mining Sciences*, 45, 831-847 (2008).

[COQU-05] Coquillay, S.: Prise en compte de la non linéarité du comportement des sols soumis à de petites déformations pour le calcul des ouvrages géotechniques. Ph.D., *Ecole National des Ponts et Chaussées* (2005).

[DAHL-09] Dahlem, E., Manhart, C., Grasset-Bourdel, R., Huger, M., Chotard, T.: Resonant frequency and damping analysis technique as a tool to investigate elastic moduli by microstructure alteration of refractories a elevated temperature. *Unified International Technical Conference on Refractories (UNITECR) 2009*, 13-16 October 2009, Salvador (Brazil).

[DIAK-07] Diakhaté, M.: Fatigue et comportement des couches d'accrochage dans les structures de chaussée. *Ph.D. Thesis*, Université de Limoges, France (2007).

[DIAK-10] Diakhaté, M., Millien, A. Petit, C. Phelipot-Mardelé, A., Pouteau B.: Experimental investigation of tack coat fatigue performance: Towards an improved lifetime assessment of pavement structure interfaces. *Construction and Building Materials*, 11 (2010).

[DRUC-52] Drucker, D.C, Prager, W.: Soil mechanics and plastic analysis or limit design. *Quaterly of Applied Mathematics*, 10, 157-165 (1952).

[HARM-94] Harmuth, H.: Investigation of the adherence and the fracture behavior of polymer cement concrete. *Cement and Concrete Research*, 25, 497-502 (1994).

[HARM-95] Harmuth, H.: Stability of crack propagation associated with fracture energy determined by wedge splitting specimen. *Theoretical and Applied Fracture Mechanics*, 23, 103-108 (1995).

[HARM-96] Harmuth, H., Rieder, K., Krobath, M., Tschegg, E.: Investigation of the nonlinear fracture behavior of ordinary ceramic refractory materials. *Materials Science and Engineering*, A214, 53-61 (1996).

[HAWO-04] Hawong, J.S., Shin, D.C., Boek, U.C.: Validation of pure shear test device using finite element method and experimental methods. *Engineering Fracture Mechanics*, 71, 233-243 (2004).

[HE-10] He, Z-J., Song, Y-P.: Triaxial strength and failure criterion of plain high-strength and high-performance concrete before and after high temperatures. *Cement and Concrete Research* (2010).

[HILL-77] Hillemeier, B., Hilsdorf, H.K.: Fracture mechanics studies on concrete compounds." *Cement and Concrete Research*, 7(5), 523–535 (1977).

[HOEK-80] Hoek, E., Brown, E.T.: Empirical Strength criterion for rock masses." *Journal of the Geotechnical Engineering Division*, ASCE, 106 (GT9), 1013-1035 (1980).

[HOSF-05] Hosford, W.F.: Mechanical behavior of materials. *Cambridge University Press* (2005).

[HUGE-07] Huger, M., Tessier-Doyen, N., Chotard, T., Gault, C.: Microstructural Effects Associated to CTE Mismatch for Enhancing the Thermal Shock Resistance of Refractories: Investigation by High Temperature Ultrasounds. Cfi/Ber. DKG 84(9), 93-103 (2007).

[IOSI-67] Iosipescu, N.: New accurate procedure for single shear testing of metals. *Journal of Materials*, 2(3), 537-566 (1967).

[KAKR-07] Kakroudi, M.G.: Comportement thermomécanique en traction de bétons réfractaires : influence de la nature des agrégats et de l'histoire thermique. Ph.D., *Université de Limoges* (2007).

[KIM-79] Kim, M.M., Ko, H.Y.: Multistage triaxial testing of rocks. *Geotechnical Testing Journal*, 2, 98-105 (1979).

[KOVA-75] Kovari, K., Tisa, A. Multiple failure state and strain controlled triaxial tests. *Rock Mechanics and Rock Engineering*, 71, 17-33 (1975).

[KRIS-10] Krishnan, A., Xu, L.R.: Effect of the interfacial stress distribution on the material interfacial shear strength measurement. *Experimental. Experimental Mechanics*, 50, 283-288 (2010).

[LECK-09] Leckie, F.A., Dal Bello, D.J.: Strength and Stiffness of Engineering Systems. *Springer Science + Business Media* (2009).

[LEE-94] Lee, Y.L.: Prise en compte des non-linearités de comportement des sols et des roches dans la modélisation du creusement d'un tunnel. Ph.D., *University of Paris* (1994).

[LINS-86] Linsbauer, H.N. Tschegg, E.K.: Fracture energy determination of concrete with cube shaped specimens. *Zement und Beton*, 31, 38-40 (1986).

[MERL-00] Merlin, L.G., Neumeister, J.M., Pettersson, K.B., Johansson, H.: Evaluation of four composite shear test methods by digital speckel strain mapping and fractographis analysis. *Journal of Composition Technology and Research*, 22(3), 161-172 (2000).

[NETZ] Netzsch RUL/CIC Apparatus 421 for the Determination of Refractoriness Under Load and Creep In Compression – product brochure.

[NEUM] Neumeister, J.M, Pettersson, K.B.: Analysis of the IDNS test for composite interlaminar shear properties. *Composition Science and Technology*, in press.

[NGUY-06] Nguyen, D.T.: Prédiction des déformations permanentes des couches de surface des chaussées bitumineuses. Ph.D., *Ecole Nationale des Ponts et Chaussées* (2006).

[NILI-05] Nilica, R., Harmuth, H.: Mechanical and fracture mechanical characterization of building materials used for external thermal insulation composite systems. *Cement and Concrete Research*, 35, 1641-1645 (2005).

[NORM-04] Norman, P.A.: *Evaluation of multistage triaxial testing on Berea sandstone* (Master's thesis). Retrieved from University of Oklahoma graduate college (2004).

[OTTO-05] Ottosen, N.S., Ristinmaa, M.:.The mechanics of constitutive modeling. *Elsevier Ldt* (2005).

[PAGO-04] Pagoulatos, A.: Evaluation of multistage triaxial testing on Berea sandstone. Ph. D., *university of Norman* (2004).

[PETT-06a] Petterson, K.B., Neumeister, J.M.: A tensile setup for the IDNS composite shear test. *Composites*, A 37, 229-242 (2006).

[PETT-06b] Pettersson, K.B., Neumeister, J.M., Gamstedt, E.K., Öberg, H.: Stiffness reduction, creep, and irreversible strains in fiber composites tested in repeated interlaminar shear. *Composite Structures*, 76, 151-161 (2006).

[ROEB-02] Roebben, G., Duan, R.G., Sciti, D., Van der Biest, O.: Assessment of the high temperature elastic and damping properties of silicon nitrides and carbides with the impulse excitation technique. *Journal of the European Ceramic Society*, 22, 2501-2509 (2002).

[SCHA-04] Schacht, C.A.: Refractories Handbook. *Mechanical engineering (Marcel Dekker, Inc.),* ISSN 0899-3858; 178 (2004).

[TESS-03] Tessier-Doyen, N.: Etude experimentale et numérique du comportement thermomécanique de matériaux réfractaires modèles. Ph.D., *Université de Limoges* (2003).

[TSCH-86] Tschegg, E.K.: Testing device and appropriate specimen shapes for tests to measure fracture values (in German). *Austrian Patent Specification AT*, 390-328 (1986).

[TSCH-09] Tschegg, E.K., Fendt, K.T., Manhart, C., Harmuth, H.: Uniaxial and biaxial fracture behavior of refractory materials. *Engineering Fracture mechanics*, 76, 2249-2259 (2009).

[XAVI-04] Xavier, J.C., Garrido, N.M., Oliviera, M., Morais, J.L., Camanho, P.P., Pierron, F.: A comparison between the Iosipescu and off-axis shear test methods for the characterization of Pinus Pinaster Ait. *Composites*, A 35, 827-840 (2004).

[YOUN-10] Youn, H., Tonon, F.: Multi-stage triaxial test on brittle rock. *International Journal of Rock Mechanics and Mining Sciences*, 47, 678-684 (2010).

[YU-10] Yu, T., Tend, J.G., Wong, Y.L., Dong, S.L.: Finite element modeling of confined concrete-I: Drucker-Prager type plasticity model. *Engineering Structures*, 32, 665-679 (2010).

Abstract

In many industrial applications, combination of compressive and shear loads will act on refractory linings. Therefore the prediction of lining failure requires the knowledge of the multiaxial behaviour of the refractory materials under service conditions. In order to take into account those aspects in modelling, Drucker-Prager criterion is often used to describe the mechanical behaviour of granular materials. It applies a linear dependency of the shear strength on the hydrostatic pressure. Therefore the Drucker-Prager failure line requires the knowledge of two essential parameters which should be determined experimentally: the cohesion (d) representing the failure shear stress without any hydrostatic pressure, and the friction angle (β) defining the increase of the failure shear stress with hydrostatic pressure. For several materials experimental data are available in literature, especially in the field of geology or civil engineering. But, unfortunately characterization techniques applied so far are operating at ambient temperature only. For refractories, cohesion and friction angle have also to be determined at elevated temperature (up to e.g. 1500°C). A simple adaptation of available experimental devices, developed for room temperature measurements, to elevated temperatures is not possible. The present work proposes a new approach to carry out such measurements in the case of refractory materials.

Keywords: Drucker-Prager, cohesion, friction angle, refractory materials, shear test.

Résumé

Dans de nombreuses applications industrielles, les matériaux réfractaires subissent des contraintes combinées de compression et de cisaillement pouvant entrainer la rupture du matériau. La prédiction de la rupture du revêtement réfractaire nécessite alors la connaissance du comportement multiaxial des matériaux réfractaires dans ces conditions d’utilisation. Afin de tenir compte de ces aspects dans la modélisation numérique, le critère de Drucker-Prager est souvent utilisé pour décrire le comportement mécanique des matériaux granulaires. En effet, le critère de Drucker-Prager correspond à une approche simple qui permet de décrire la dépendance de la contrainte à rupture en cisaillement en fonction de la pression hydrostatique. Néanmoins, l’utilisation de ce critère nécessite la connaissance de deux paramètres essentiels qui doivent être déterminés expérimentalement : la cohésion (d) traduisant la contrainte à la rupture en cisaillement sans pression hydrostatique appliquée, et l’angle de frottement (β) traduisant l’évolution de cette contrainte à rupture lorsque la pression hydrostatique augmente. De nombreux travaux expérimentaux sur ce type de caractérisation sont disponibles dans la littérature, en particulier dans le domaine de la géologie ou du génie civil. Mais, malheureusement, tous ces travaux traitent de techniques de caractérisation fonctionnant à température ambiante. Dans notre cas, la cohésion et l’angle de frottement doivent aussi être déterminés à haute température (jusqu’à 1500°C). La transposition à haute température des dispositifs développés pour des mesures à température ambiante, est tout simplement impossible. Ce travail propose donc une nouvelle approche pour réaliser de telles mesures dans le cas des matériaux réfractaires.

Mots-clés : Drucker-Prager, cohésion, angle de frottement, matériaux réfractaires, essai de cisaillement.